20

Critical Exponents from Other Expansions

It is useful to compare the results obtained so far with other approaches to the critical exponents. One is a similar field-theoretic approach based on perturbation expansions of ϕ^4-theories. But instead of working in $D = 4-\varepsilon$ dimensions and continuing the results to $\varepsilon = 1$ to obtain critical exponents in the physical dimension $D = 3$, perturbation expansions can be derived directly in three dimensions, and studied in the regime of small masses. Fundamentally, this approach is less satisfactory than the previous one since there is no small parameter analogous to ε which permits us to prove the existence of a scaling limit at least for small ε. Another disadvantage is that it is impossible to calculate the expansion coefficients analytically, except for one- and two loop-diagrams. In one respect the three-dimensional approach has, however, an advantage: the power series have long been available up to six loops for ω, η, and ν, and there exist recent results up to seven loops for the critical exponents η and ν. Although numerical expansions are not as esthetic as the exact expansions derived in this book, their increased order leads to a higher accuracy in the critical exponents, as we shall see below in Section 20.4.

Another approach is based on *high-temperature expansions* for lattice models of the O(N)-symmetric classical Heisenberg model with the energy of Eq. (1.52). The critical exponents will be derived from such expansions in Section 20.8.

Finally we take advantage of the fact that the O(N)-symmetric classical Heisenberg model is exactly solvable in the limit of large N, where it reduces to the spherical model [recall the remark after Eq. (1.69)]. It is therefore possible to expand the ϕ^4-theory around this limit in powers of $1/N$. The results will be compared with those from the perturbation expansions in Section 20.2.

20.1 Sixth-Order Expansions in Three Dimensions

The three-dimensional ϕ^4-theory is defined by the bare energy functional

$$E[\phi_B] = \int d^D x \left\{ \frac{1}{2} \left[\partial \phi_B(\mathbf{x})\right]^2 + \frac{1}{2} m_B^2 \phi_B^2(\mathbf{x}) + \frac{48\pi}{N+8} \frac{g_B}{4!} \left[\phi_B^2(\mathbf{x})\right]^2 \right\}, \tag{20.1}$$

where the coupling constant is normalized to obtain the most convenient perturbation expansions. The field $\phi_B(\mathbf{x})$ is an N-dimensional vector, and the action is O(N)-symmetric in this vector space.

By calculating the Feynman diagrams up to six loops, and imposing the normalization conditions (9.23), (9.24), and (9.33) we find renormalized values of mass, coupling constant, and field related to the bare input quantities by renormalization constants Z_ϕ, Z_{m^2}, Z_g:

$$m_B^2 = m^2 \; Z_{m^2} Z_\phi^{-1}, \quad g_B = g \, Z_g Z_\phi^{-2}, \quad \phi_B = \phi \; Z_\phi^{1/2}. \tag{20.2}$$

The divergences are removed by analytic regularization [1]. In the literature, we find expansions for m_B^2/m^2, g_B/g, and ϕ_B/ϕ in powers of g up to g^6 (six loops), the latter two having recently been extended to the power g^7 (seven loops) [2, 3]. We shall first discuss in detail the variational resummation of the six-loop expansions.. The small improvements of the critical exponents brought about by the seven-loop terms will be calculated separately in Section 20.4.

Introducing the reduced dimensionless coupling constants $\bar{g} \equiv g/m$ and $\bar{g}_B \equiv g_B/m$, these determine the renormalization group functions by the following equations:

$$\omega(\bar{g}) = \frac{d\beta(\bar{g})}{d\bar{g}}, \quad \beta(\bar{g}) = -\left\{\frac{d}{d\bar{g}}\log\frac{\bar{g}Z_g}{Z_\phi^2}\right\}^{-1} = -\bar{g}_B\left(\frac{d\bar{g}_B}{d\bar{g}}\right)^{-1}, \tag{20.3}$$

$$\eta(\bar{g}) = \beta(\bar{g})\frac{d}{d\bar{g}}\log Z_\phi = \beta(\bar{g})\frac{d}{d\bar{g}}\log\frac{\phi_B^2}{\phi^2}, \tag{20.4}$$

$$\eta_m(\bar{g}) = -\beta(\bar{g})\frac{d}{d\bar{g}}\log\frac{Z_{m^2}}{Z_\phi} = -\beta(\bar{g})\frac{d}{d\bar{g}}\log\frac{m_B^2}{m^2}. \tag{20.5}$$

For our purpose, we must study all quantities as functions of the reduced bare coupling constant $\bar{g}_B$. In terms of this variable, the beta function $\beta(\bar{g})$ is obtained from the logarithmic derivative

$$\beta(\bar{g}_B) = -\frac{d\bar{g}(\bar{g}_B)}{d\log\bar{g}_B} = -\bar{g}_B\bar{g}'(\bar{g}_B). \tag{20.6}$$

The function $\omega(\bar{g}_B)$ may then be obtained from the function $\bar{g} = \bar{g}(\bar{g}_B)$ by the logarithmic derivative

$$\omega(\bar{g}_B) = -\frac{d\log\beta(\bar{g}_B)}{d\log\bar{g}_B} = -\frac{d\log[\bar{g}_B\bar{g}'(\bar{g}_B)]}{d\log\bar{g}_B} = -1 - \bar{g}_B\frac{\bar{g}''(\bar{g}_B)}{\bar{g}'(\bar{g}_B)}. \tag{20.7}$$

Comparison with Eq. (20.21) shows that if $\bar{g}(\bar{g}_B)$ goes to a constant $\bar{g}^*$ in the strong-coupling limit $\bar{g}_B \to \infty$, the limiting value $\omega \equiv \omega(\infty)$ plays the role of the approach parameter $2/q$ of the strong-coupling expansion of the function $\bar{g}(\bar{g}_B)$.

Similarly we convert Eqs. (20.4) and (20.5) into functions of the bare coupling constant g_B:

$$\eta_m(\bar{g}_B) = -\frac{d}{d\log\bar{g}_B}\log\frac{m^2}{m_B^2}, \qquad \eta(\bar{g}_B) = \frac{d}{d\log\bar{g}_B}\log\frac{\phi^2}{\phi_B^2}, \tag{20.8}$$

which correspond to the relations (19.67) in $4-\varepsilon$ dimensions. If $\eta_m(\bar{g}_B)$ and $\eta(\bar{g}_B)$ have finite strong-coupling limits $\eta_m = \eta_m(\infty)$ and $\eta = \eta(\infty)$, these equations imply the strong-coupling behaviors

$$\frac{m^2}{m_B^2} \propto \bar{g}_B^{-\eta_m}, \qquad \frac{\phi^2}{\phi_B^2} \propto \bar{g}_B^{\eta}, \tag{20.9}$$

corresponding to (19.68) in $4-\varepsilon$ dimensions. By replacing the reduced coupling constant $\bar{g}_B$ by g_B/m, this implies the small-mass behavior at a fixed bare coupling g_B:

$$\frac{m^2}{m_B^2} = \text{const} \times m^{\eta_m}, \qquad \frac{\phi^2}{\phi_B^2} = \text{const} \times m^{-\eta}. \tag{20.10}$$

The six-loop expansions are the following:

$$\omega(\bar{g}) = -1 + 2\bar{g}\,(8+N) - 3\bar{g}^2\,(760/27 + 164N/27) + 4\bar{g}^3\left(199.640417 + 54.94037698N + 1.34894276N^2\right)$$

$$
\begin{aligned}
&+ 5\bar{g}^4\left(-1832.206732 - 602.5212305N - 35.82020378N^2 + 0.15564589N^3\right)\\
&+ 6\bar{g}^5\left(20770.17697 + 7819.564764N + 668.5543368N^2 + 3.2378762N^3 + 0.05123618N^4\right)\\
&+ 7\bar{g}^6\left(-271300.0372 - 114181.4357N - 12669.22119N^2\right.\\
&\quad\left. - 265.8357032N^3 + 1.07179839N^4 + 0.02342417N^5\right) \qquad (20.11)\\
\eta(\bar{g}) &= \bar{g}^2\,(16/27 + 8N/27) + \bar{g}^3\left(0.3949440224 + 0.246840014N + 0.0246840014N^2\right)\\
&+ \bar{g}^4\left(6.512109933 + 4.609221057N + 0.6679859202N^2 - 0.0042985626N^3\right)\\
&+ \bar{g}^5\left(-21.64720643 - 15.1880934N - 1.891139282N^2 + 0.1324510614N^3 - 0.0065509222N^4\right)\\
&+ \bar{g}^6\left(369.7130739 + 300.7208933N + 64.07744656N^2\right.\\
&\quad\left. + 3.054030987N^3 - 0.0203994485N^4 - 0.0055489202N^5\right) \qquad (20.12)\\
\eta_m(\bar{g}) &= \bar{g}\,(2+N) - \bar{g}^2\,(92/27 + 46N/27) + \bar{g}^3\left(18.707787762 + 12.625201157N + 1.6356536385N^2\right)\\
&+ \bar{g}^4\left(-134.28726152 - 98.33833174N - 15.117303198N^2 + 0.2400236453N^3\right)\\
&+ \bar{g}^5\left(1318.4281763 + 1046.8184247N + 209.71327323N^2 + 8.143135609N^3 + 0.0937915707N^4\right)\\
&+ \bar{g}^6\left(-15281.544489 - 12918.644832N - 2980.2279474N^2\right.\\
&\quad\left. - 164.6575873N^3 + 3.0931477063N^4 + 0.0495801299N^5\right). \qquad (20.13)
\end{aligned}
$$

Here and in the subsequent set of perturbative expansions, we save space by omitting in each term $\bar{g}^n$ a denominator $(N+8)^n$.

By integrating (20.3), we see that $\omega(\bar{g})$ implies the relation between bare and renormalized coupling constant:

$$
\begin{aligned}
\bar{g}_B = \bar{g}\big[1 &+ \bar{g}\,(8+N) + \bar{g}^2\,\left(1348/27 + 350N/27 + N^2\right)\\
&+ \bar{g}^3\,\left(315.8307562667 + 120.7825947383N + 17.3632278267N^2 + N^3\right)\\
&+ \bar{g}^4\,\left(1813.1642655362 + 949.9400421368N + 203.4347168377N^2 + 21.5210551192N^3 + N^4\right)\\
&+ \bar{g}^5\,\left(11664.58684418 + 7259.6266136476N + 1965.0940131759N^2\right.\\
&\quad\left. + 298.9857773851N^3 + 25.5436671032N^4 + N^5\right)\\
&+ \bar{g}^6\,\left(57253.8939657167 + 47753.8060061961N + 16981.2530394653N^2 + 3357.7450242179N^3\right.\\
&\quad\left. + 407.679442164N^4 + 29.4800395765N^5 + N^6\right)\big]. \qquad (20.14)
\end{aligned}
$$

This can be inverted to

$$
\begin{aligned}
\bar{g} = \bar{g}_B\big[1 &- \bar{g}_B\,(8+N) + \bar{g}_B^2\,\left(2108/27 + 514N/27 + N^2\right)\\
&+ \bar{g}_B^3\,\left(-878.7937193 - 312.63444671N - 32.54841303N^2 - N^3\right)\\
&+ \bar{g}_B^4\,\left(11068.06183 + 5100.403285N + 786.3665699N^2 + 48.21386744N^3 + N^4\right)\\
&+ \bar{g}_B^5\,\left(-153102.85023 - 85611.91996N - 17317.702545N^2 - 1585.1141894N^3 - 65.82036203N^4 - N^5\right)\\
&+ \bar{g}_B^6\,\left(2297647.148 + 1495703.313\,N + 371103.0896N^2 + 44914.04818N^3\right.\\
&\quad\left. + 2797.291579N^4 + 85.21310501N^5 + N^6\right)\big], \qquad (20.15)
\end{aligned}
$$

where we suppress a denominator $(N+8)^n$ in each term $\bar{g}_B^n$. Inserting this into the functions (20.11), (20.12), and (20.13), they become

$$
\begin{aligned}
\omega(\bar{g}_B) &= -1 + 2\bar{g}_B\,(8+N) - \bar{g}_B^2\,\left(1912/9 + 452N/9 + 2N^2\right)\\
&+ \bar{g}_B^3\,\left(3398.857964 + 1140.946693N + 95.9142896N^2 + 2N^3\right)\\
&+ \bar{g}_B^4\,\left(-60977.50127 - 26020.14956N - 3352.610678N^2 - 151.1725764N^3 - 2N^4\right)\\
&+ \bar{g}_B^5\,\left(1189133.101 + 607809.998N + 104619.0281N^2 + 7450.143951N^3 + 214.8857494N^4 + 2N^5\right)\\
&+ \bar{g}_B^6\,\left(-24790569.76 - 14625241.87N - 3119527.967N^2\right.\\
&\quad\left. - 304229.0255N^3 - 14062.53135N^4 - 286.3003674N^5 - 2N^6\right), \qquad (20.16)\\
\eta(\bar{g}_B) &= \bar{g}_B^2\,\left(16/27 + 8N/27\right) + \bar{g}_B^3\,\left(-9.086537459 - 5.679085912N - 0.5679085912N^2\right)\\
&+ \bar{g}_B^4\,\left(127.4916153 + 94.77320534N + 17.1347755N^2 + 0.8105383221N^3\right)
\end{aligned}
$$

$$
\begin{aligned}
&+ \bar{g}_B^5 \left(-1843.49199 - 1576.46676N - 395.2678358N^2 - 36.00660242N^3 - 1.026437849N^4\right) \\
&+ \bar{g}_B^6 \left(28108.60398 + 26995.87962N + 8461.481806N^2 + 1116.246863N^3\right. \\
&\qquad \left. + 62.8879068N^4 + 1.218861532N^5\right) \qquad (20.17)\\
\eta_m(\bar{g}_B) &= \bar{g}_B\,(2+N) - \bar{g}_B^2\,\left(-524/27 - 316N/27 - N^2\right) \\
&+ \bar{g}_B^3\,\left(229.3744544 + 162.8474234N + 26.08009809N^2 + N^3\right) \\
&+ \bar{g}_B^4\,\left(-3090.996037 - 2520.848751N - 572.3282893N^2 - 44.32646141N^3 - N^4\right) \\
&+ \bar{g}_B^5\,\left(45970.71839 + 42170.32707N + 12152.70675N^2 + 1408.064008N^3 + 65.97630108N^4 + N^5\right) \\
&+ \bar{g}_B^6\,\left(-740843.1985 - 751333.064N - 258945.0037N^2 - 39575.57037N^3\right. \\
&\qquad \left. - 2842.8966N^4 - 90.7145582N^5 - N^6\right). \qquad (20.18)
\end{aligned}
$$

Let us also write down a power series expansion for the function $\gamma(g_B) = [2-\eta(g_B)]/[2-\eta_m(g_B)]$ which tends to the critical exponent γ of susceptibility. In resummation procedures applied to functions of the renormalized coupling constant g, this series has always been favored over that for $\eta(g)$ since, in contrast to $\eta(g)$, its expansion coefficients of $\gamma(g)$ have alternating signs permitting application of Padé-Borel resummation techniques [4]. Note, however, that the expansion (20.17) in powers of $\bar{g}_B$ does have alternating signs. For $\gamma(g_B)$, the series reads

$$
\begin{aligned}
\gamma(\bar{g}_B) &= 1 + \bar{g}_B\,(2+N)\,/2 + \bar{g}_B^2\,\left(-9 - 5N - N^2/4\right) \\
&+ \bar{g}_B^3\,\left(100.5267922 + 64.05955095N + 7.148077413N^2 + 0.125N^3\right) \\
&+ \bar{g}_B^4\,\left(-1306.696473 - 953.5355208N - 165.6165894N^2 - 7.886473674N^3 - 0.0625N^4\right) \\
&+ \bar{g}_B^5\,\left(19047.24345 + 15717.20743N + 3667.58258N^2 + 300.9668324N^3 + 7.848484825N^4 + 0.03125N^5\right) \\
&+ \bar{g}_B^6\,\left(-304324.882 - 279842.9929N - 81107.12259N^2 - 9519.124419N^3 - 457.7147389N^4\right. \\
&\qquad \left. - 7.463312096N^5 - 0.015625N^6\right). \qquad (20.19)
\end{aligned}
$$

20.2 Critical Exponents up to Six Loops

We are now ready to apply our strong-coupling theory to these expansions. First we study the $\bar{g}_B \to \infty$ -limit of the series (20.15) for the renormalized reduced coupling constant $\bar{g}$. We expect the theory to reproduce experimentally observed scaling laws which means that $\bar{g}(\bar{g}_B)$ should tend to some constant value: $\bar{g}(\bar{g}_B) \to \bar{g}^*$ for $\bar{g}_B \to \infty$. The leading power parameter $p/q = s$ in $\bar{g}_B$ must be set equal to zero, implying for the power series of $\bar{g}(\bar{g}_B)$ the vanishing of the logarithmic derivative in the strong-coupling limit, as before in Eq (19.64):

$$
0 = \bar{g}_B \frac{\bar{g}'(\bar{g}_B)}{\bar{g}(\bar{g}_B)}\bigg|_{\bar{g}_B=\infty}. \qquad (20.20)
$$

This equation is used to determine the critical exponent $\omega = 2/q$.

Alternatively, we may determine ω from the strong-coupling limit of the self-consistency condition Eq. (19.65) for ω, which reads here

$$
\omega = -1 - \bar{g}_B \frac{\bar{g}''(\bar{g}_B)}{\bar{g}'(\bar{g}_B)}\bigg|_{\bar{g}_B=\infty}. \qquad (20.21)
$$

We now insert the expansion (20.15) for $\bar{g}(\bar{g}_B)$ into Eq. (20.20), re-expand up to order $\bar{g}_B^7$, and resum the series by variational perturbation theory. for increasing orders L. The zeros determine the successive approximations ω_L for $L = 3, 4, 5, 6$. This is done for O(N)-symmetric

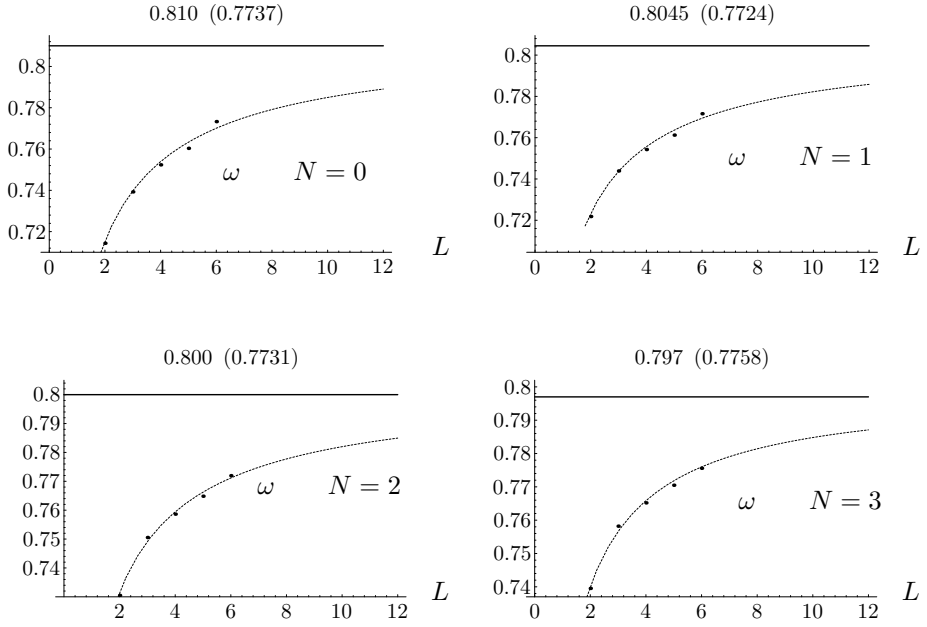

FIGURE 20.1 Behavior of strong-coupling values $\omega = \omega(\infty)$ with increasing order L of the approximation, for O(N)-symmetric theories with $N = 0,\ 1,\ 2,\ 3,\ \ldots$. These are the critical exponents observable in the approach to scaling of the second-order phase transitions in dilute polymer solutions, Ising magnets, superfluid helium, and the classical Heisenberg model. The points are fitted by $\omega - b\, e^{-cL^{1-\omega}}$ (dashed line), determining by extrapolation the limiting values indicated by the horizontal lines, which are plotted in the first plot of Fig. 20.2 and listed in Table 20.1 on page 375. The highest approximation ω_6 is indicated on top of the line in parentheses.

theories with $N = 0,\ 1,\ 2,\ 3,\ \ldots$. The values of the highest available approximation ω_6 are found in the parentheses of the last column of Table 20.1 on page 375.

Since L is not very large, the results require extrapolation to infinite L. The functional form of the L-dependence was determined in (19.51), predicting the large-L behavior

$$\omega_L \approx \omega - b\, e^{-cL^{1-\omega}}. \tag{20.22}$$

In the upper left-hand plot of Fig. 20.1 we illustrate how the successive approximations ω_2—ω_6 are fitted by this asymptotic curve for O(N)-theories with $N = 0$ (dilute polymer solutions), $N = 1$, (Ising), $N = 2$ (superfluid helium), $N = 3$ (classical Heisenberg model). The extrapolated values obtained by such fits for infinite L are shown in the last column of Table 20.1 on page 375. They are plotted in the first plot of Fig. 20.2, together with the sixth-order approximation to show the significance of the $L \to \infty$ -extrapolation.

Our numbers merge smoothly with the $1/N$-expansion curve which has been calculated [5] to order $1/N^2$:

$$\omega = 1 - 8\,\frac{8}{3\pi^2}\frac{1}{N} + 2\left(\frac{104}{3} - \frac{9}{2}\pi^2\right)\left(\frac{8}{3\pi^2}\frac{1}{N}\right)^2 + \mathcal{O}(N^{-3}). \tag{20.23}$$

To judge the internal consistency of our procedure, we calculate ω once more from Eq. (20.21) for $\omega = 2/q$. Since ω appears also on the right-hand side of the series via the parameter q, this represents a self-consistency relation which can be iterated until input and output values for ω coincide for each L. The results are shown in Fig. 20.3 for increasing orders

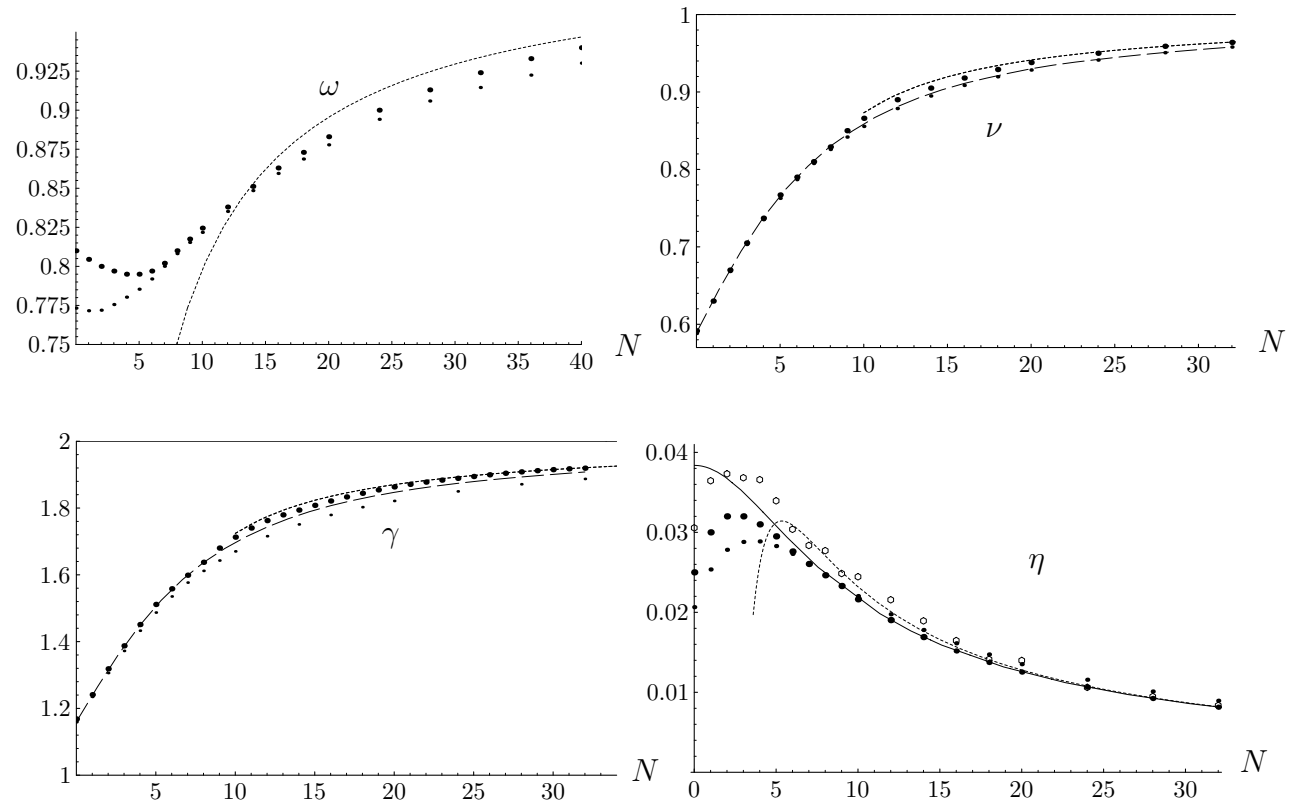

FIGURE 20.2 Sixth-order approximations to $\omega, \nu, \gamma, \eta$ (thin dots), and their $L \to \infty$ -limit (fat dots). The dashed lines in the second and third figures are an interpolation to the Padé-Borel resummations of S.A. Antonenko and A.I. Sokolov, Phys. Rev. E *51*, 1894 (1995) (where ω was not calculated). Their data for η scatter too much to be represented in this way—they are indicated by small circles. The dotted curves show $1/N$ -expansions for all four quantities. Note that our results lie closer to these than those of S.A. Antonenko and A.I. Sokolov. The solid η-curve is explained after Eq. (20.27).

$L = 2,\ 3,\ 4,\ 5,\ 6$, in the Ising case $N = 1$. The data points are again fitted with the functional behavior (20.22), imposing the same extrapolated $\omega(\infty)$-values as in the previous fits.

The critical exponent ω can also be calculated from the expansions for γ and ν in this self-consistent way, as shown in Fig. 20.4.

Note that the agreement between the self-consistent ω-values with the previous ones determined from the $p = 0$ -condition can be considered as a confirmation of the hypothesis that the theory does indeed have a definite strong-coupling limit in which $\bar{g}(\bar{g}_B)$ tends to a constant $\bar{g}^*$ (an *infrared-stable fixed point* in the language of the renormalization group). It also implies all other scaling properties to be derived below.

Proceeding to other critical exponents, we now take the function $\nu^{-1}(\bar{g}_B) = 2 - \eta_m(\bar{g}_B)$ to the strong-coupling limit, to determine $\nu = \nu(\infty)$. The extrapolations to large L are done with the help of the approximations $\nu_2,\ \nu_3, \ldots, \nu_6$, as illustrated in Fig. 20.5. The resulting critical exponents are plotted against N in the second plot of Fig. 20.2, and listed in Table 20.1 on page 375. The points are seen to merge well with those of the $1/N$ -expansion [5] for ν:

$$\nu \;=\; 1 - 4\,\frac{8}{3\pi^2}\frac{1}{N} + \left(\frac{56}{3} - \frac{9}{2}\pi^2\right)\left(\frac{8}{3\pi^2}\frac{1}{N}\right)^2 + \mathcal{O}(N^{-3}). \tag{20.24}$$

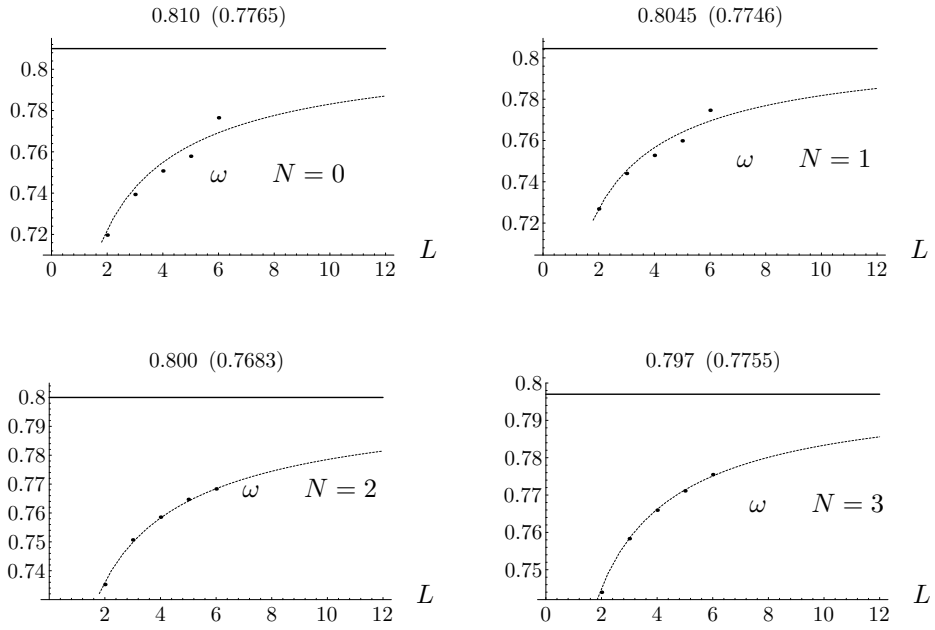

FIGURE 20.3 Behavior of self-consistent strong-coupling values $\omega = \omega(\infty)$ from Eq. (20.21) for $2/q = \omega$ with increasing order L of the approximation, for O(N)-symmetric theories with $N = 0,\ 1,\ 2,\ 3,\ \ldots$.

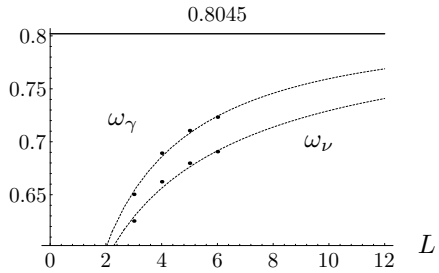

FIGURE 20.4 The ω-exponents obtained from the expansions of γ and ν for $N = 1$. Their convergence is much slower.

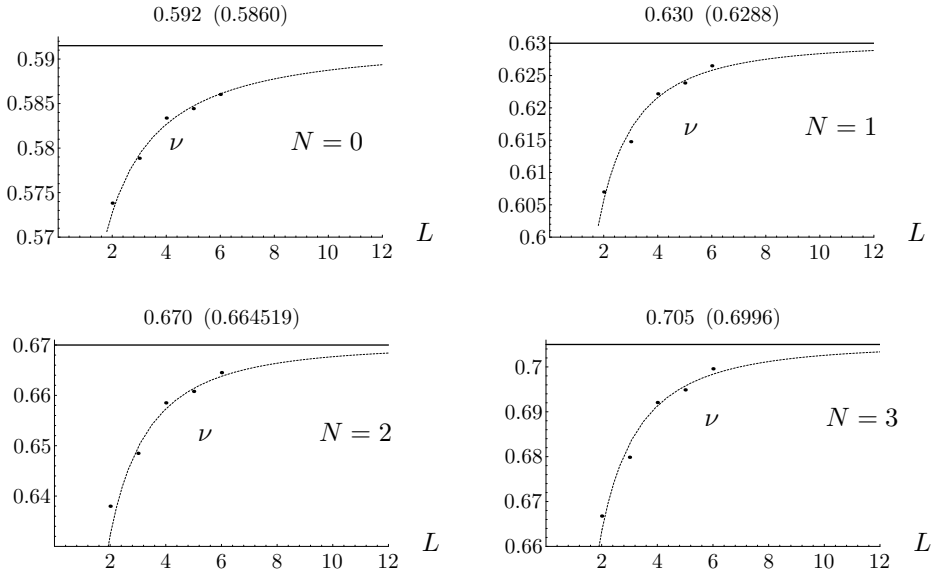

FIGURE 20.5 Plot analogous to Fig. 20.1 of critical exponent $\nu = \nu(\infty)$, illustrating the extrapolation procedure to $L \to \infty$ for $N = 0,\ 1,\ 2,\ 3$. The results of the extrapolation are plotted against L in the second plot of Fig. 20.2 and listed in Table 20.1 on page 375.

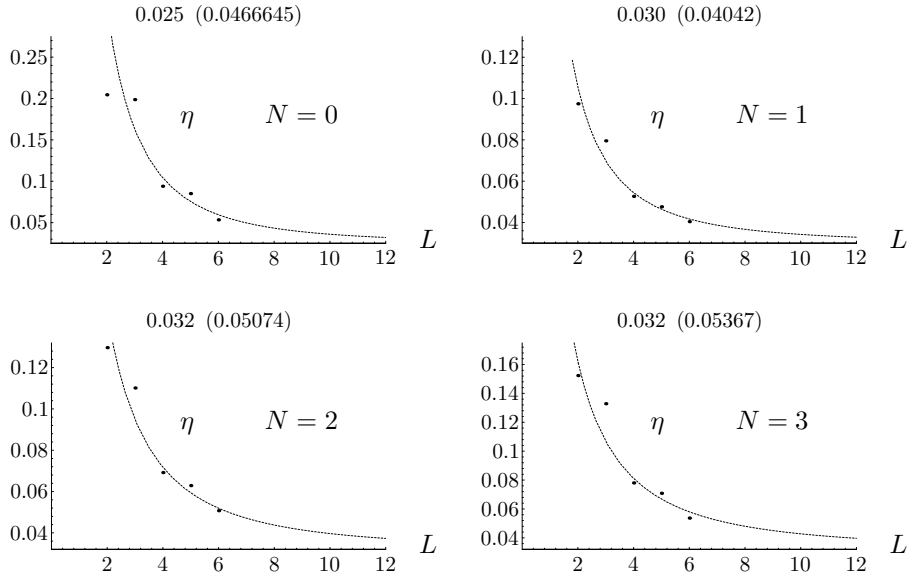

FIGURE 20.6 Plot analogous to Fig. 20.1 of critical exponent $\eta = \eta(\infty)$, illustrating the extrapolation procedure to $L \to \infty$ for $N = 0,\ 1,\ 2,\ 3$. The results of the extrapolation are plotted against N in the fourth plot of Fig. 20.2 and listed in Table 20.1 on page 375.

The function $\gamma(\bar{g}_B)$ is treated somewhat differently. Since γ serves to determine the critical exponent η via the scaling relation $\eta = 2 - \gamma/\nu$, and since this combination is very sensitive to small errors in γ (and in ν), we proceed as follows. After applying our method to the γ-series and calculating the approximations $\gamma_2,\ \gamma_3, \ldots, \gamma_6$, we go over to $\eta_2,\ \eta_3, \ldots, \eta_6$ via the scaling relation $\eta_L = 2 - \gamma_L/\nu$ and perform the extrapolation $L \to \infty$ on these η-values, as illustrated in Fig. 20.6. In this way, we obtain the smooth η-curves shown in the fourth plot of Fig. 20.2 and listed in Table 20.1 on page 375. The values of the highest approximation η_6 in the parentheses of Table 20.1 are obtained from a direct variational treatment of the perturbation expansion for η. These are closer to the final η-values than the approximations of $\eta_6 = 2 - \gamma_6/\nu$ used for the extrapolation, which are indicated in the parentheses on top of the plots of Fig. 20.6. Still, we have used the latter for extrapolation since there are five of them to be fitted with the asymptotic curve (20.22), while the η-expansion which has no linear term in $\hat{g}_B$ provides us only with four values, making a fit less reliable.

The extrapolated η-values are inserted into the scaling relation $\gamma = \nu(2 - \eta)$ to derive the extrapolated γ-values plotted in the third plot of Fig. 20.2 and listed in Table 20.1 on page 375. A direct extrapolation $L \to \infty$ of the variational. approximations γ_L to the γ-expansion turns out to be fully compatible with the previous ones, as illustrated in Fig. 20.7.

For large N, our critical exponents η are in excellent agreement with the $1/N$ -expansion, which is known [5, 6] up to order $1/N^3$:

$$\eta = \frac{8}{3\pi^2}\frac{1}{N} - \frac{8}{3}\left(\frac{8}{3\pi^2}\frac{1}{N}\right)^2 - \left[\frac{797}{18} - \left(27\log 2 - \frac{61}{4}\right)\zeta(2) + \frac{189}{4}\zeta(3)\right]\left(\frac{8}{3\pi^2}\frac{1}{N}\right)^3 + \mathcal{O}(N^{-4}), \tag{20.25}$$

where $\zeta(z)$ is Riemann's zeta function (13.16). Note that for η the finite-N corrections are very small. In fact, from the η_6-values near $N = 1000$, we can extract numerically the $1/N$-expansion

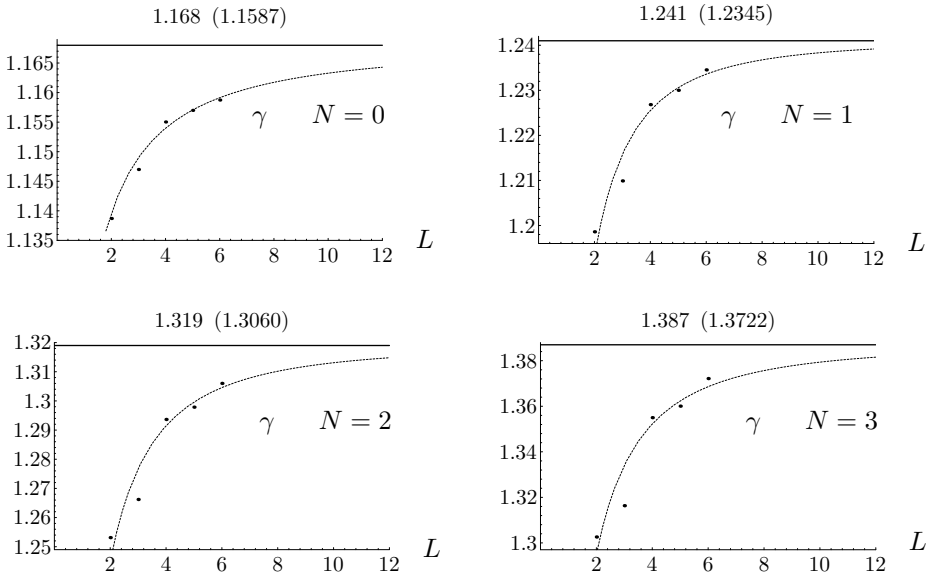

FIGURE 20.7 Plot analogous to Fig. 20.1 of critical exponent $\gamma = \gamma(\infty)$, illustrating the extrapolation procedure to $L \to \infty$ for $N = 0,\ 1,\ 2,\ 3$. The results of the extrapolation are plotted against N in the third plot of Fig. 20.2 and listed in Table 20.1 on page 375.

$$\eta \approx 0.303\,\frac{1}{N} - 0.104\,\frac{1}{N^2}, \tag{20.26}$$

which agrees reasonably well with the exact expansion

$$\eta \approx 0.270\,\frac{1}{N} - 0.195\,\frac{1}{N^2}. \tag{20.27}$$

It is worth pointing out that we may also apply our strong-coupling theory to $1/N$ -expansions for η, to find expressions valid for all N down to $N = 0$ by treating $1/N$ just like the variable g_B in Section 19.1. Taking the $1/N$-expansion as an example, we derive a smooth fit from large to rather small N by adding another term $-104/N^4$ to (20.25) before going through the resummation. The extra term improves the fit, such that it is probably a good prediction for the yet unknown next term in the $1/N$-expansion.

Since η starts out linearly at the "strong-coupling" value $1/N = \infty$, the parameters p and q are 0 and 2, respectively. The resulting curve is shown in the fourth plot of Fig. 20.2. It fits all data except for very small N. The figure shows also successive approximations provided by the $1/N$-expansion.

The exponents γ also merge well with their $1/N$-expansion [7]

$$\gamma = 2 - 9\,\frac{8}{3\pi^2}\frac{1}{N} + \left(44 - 9\pi^2\right)\left(\frac{8}{3\pi^2}\frac{1}{N}\right)^2 + \mathcal{O}(N^{-3}), \tag{20.28}$$

as seen in the third plot of Fig. 20.2.

Finally, we exhibit the full power of our theory by plotting for the Ising case $N = 1$ the functions $\bar{g}(\bar{g}_B)$, $\omega(\bar{g}_B)$, $\nu(\bar{g}_B)$, $\eta(\bar{g}_B)$ for all coupling strengths in Figs. 20.8–20.10, together with the diverging perturbative approximations as well as the convergent strong-coupling expansion. We do this successively for each increasing order L of the approximations. On a logarithmic plot, the quality of these very different approximations looks surprisingly similar.

Although the functions $\bar{g}(\bar{g}_B)$, $\omega(\bar{g}_B)$, $\nu(\bar{g}_B)$, $\eta(\bar{g}_B)$ in Figs. 20.8–20.10 are derived by a numerical variational procedure, it is possible to write the results down in the form of new strong-coupling expansions which converge for *all* coupling strengths. We shall demonstrate

TABLE 20.1 Critical exponents of Ref. [8] in comparison with those obtained by Padé-Borel resummation in Ref. [3], as well as earlier results (all cited in Notes and References). They refer to six-loop expansions in $D = 3$ dimensions ([2, 9]), or to five-loop expansions in $\epsilon = 4 - D$ ([10, 11]). For each of our results we give the $L = 6$ -approximation in parentheses to display the importance of the extrapolation procedure $L \to \infty$.

N	g_c	$\gamma(\gamma_6)$	$\eta(\eta_6)$	$\nu(\nu_6)$	α	β	ω (ω_6)	
0		1.168(1.159)	0.025(0.0206)	0.592(0.586)			0.810(0.7737)	
	1.402	1.160	0.034	0.589	0.231	0.305		[3]
	1.421±0.004	1.161±0.003	0.026±0.026	0.588±0.001	0.236±0.004	0.302±0.004	0.794 ± 0.06	[2]
	1.421 ± 0.008	1.1615 ± 0.002	0.027 ± 0.004	0.5880±0.0015		0.3020±0.0015	0.80 ± 0.04	[9]
		1.160 ± 0.004	0.031 ± 0.003	0.5885±0.0025		0.3025±0.0025	0.82 ± 0.04	[11]
1		1.241(1.235)	0.030(0.0254)	0.630(0.627)			0.805(0.7724)	
	1.419	1.239	0.038	0.631	0.107	0.327	0.781	[3]
	1.416±0.0015	1.241±0.004	0.031±0.011	0.630±0.002	0.110±0.008	0.324 ± 0.06	0.788±0.003	[2]
	1.416±0.004	1.2410±0.0020	0.031±0.004	0.6300±0.0015		0.3250±0.0015	0.79±0.03	[9]
			0.035 ± 0.002	0.628±0.001			0.80 ± 0.02	[10]
		1.1239 ± 0.004	0.037 ± 0.003	0.6305±0.0025		0.3265±0.0025	0.81 ± 0.04	[11]
2		1.318(1.306)	0.032(0.0278)	0.670(0.665)			0.800(0.7731)	
	1.408	1.315	0.039	0.670	-0.010	0.348	0.780	[3]
	1.406±0.005	1.316±0.009	0.032±0.015	0.669±0.003	-0.007±0.009	0.346±0.009	0.78 ± 0.01	[2]
	1.406±0.004	1.3160±0.0025	0.033±0.004	0.6690±0.0020		0.3455±0.002	0.78±0.025	[9]
			0.037 ± 0.002	0.665±0.001			0.79 ± 0.02	[10]
		1.315 ± 0.007	0.040 ± 0.003	0.671±0.005		0.3485±0.0035	0.80 ± 0.04	[11]
3		1.387(1.372)	0.032(0.0288)	0.705(0.700)			0.797(0.7758)	
	1.392	1.386	0.038	0.706	-0.117	0.366	0.780	[3]
	1.392±0.009	1.390±0.01	0.031±0.022	0.705±0.005	-0.115±0.015	0.362	0.78 ± 0.02	[2]
	1.391 ±0.004	1.386±0.004	0.033±0.004	0.705±0.003		0.3645±0.0025	0.78 ± 0.02	[9]
			0.037 ± 0.002	0.79±0.02			0.79 ± 0.02	[10]
		1.390 ± 0.010	0.040 ± 0.003	0.710±0.007		0.368±0.004	0.79 ± 0.04	[11]
4		1.451(1.433)	0.031(0.0289)	0.737(0.732)			0.795(0.780)	
	1.375	1.449	0.036	0.738	-0.213	0.382	0.783	[3]
5		1.511(1.487)	0.0295(0.0283)	0.767(0.760)			0.795(0.785)	
	1.357	1.506	0.034	0.766	-0.297	0.396	0.788	[3]
6		1.558(1.535)	0.0276(0.0273)	0.790(0.785)			0.797(0.792)	
	1.339	1.556	0.031	0.790	-0.370	0.407	0.793	[3]
7		1.599(1.577)	0.0262(0.0260)	0.810(0.807)			0.802(0.800)	
	1.321	1.599	0.029	0.811	-0.434	0.417	0.800	[3]
8		1.638(1.612)	0.0247(0.0246)	0.829(0.825)			0.810(0.808)	
	1.305	1.637	0.027	0.830	-0.489	0.426	0.808	[3]
9		1.680(1.643)	0.0233(0.0233)	0.850(0.841)			0.817(0.815)	
	1.289	1.669	0.025	0.845	-0.536	0.433	0.815	[3]
10		1.713(1.670)	0.0216(0.0220)	0.866(0.854)			0.824(0.822)	
	1.275	1.697	0.024	0.859	-0.576	0.440	0.822	[3]
12		1.763(1.716)	0.0190(0.0198)	0.890(0.877)			0.838(0.835)	
	1.249	1.743	0.021	0.881	-0.643	0.450	0.836	[3]
14		1.795(1.750)	0.0169(0.0178)	0.905(0.894)			0.851(0.849)	
	1.227	1.779	0.019	0.898	-0.693	0.457	0.849	[3]
16		1.822(1.779)	0.0152(0.0161)	0.918(0.907)			0.862(0.860)	
	1.208	1.807	0.017	0.911	-0.732	0.463	0.861	[3]
18		1.845(1.803)	0.0148(0.0137)	0.929(0.918)			0.873(0.869)	
	1.191	1.829	0.015	0.921	-0.764	0.468	0.871	[3]
20		1.864(1.822)	0.0125(0.0135)	0.938(0.927)			0.883(0.878)	
	1.177	1.847	0.014	0.930	-0.789	0.471	0.880	[3]
24		1.890(1.850)	0.0106(0.0116)	0.950(0.939)			0.900(0.894)	
	1.154	1.874	0.012	0.942	-0.827	0.477	0.896	[3]
28		1.909(1.871)	0.009232(0.01010)	0.959(0.949)			0.913(0.906)	
	1.136	1.893	0.010	0.951	-0.854	0.481	0.909	[3]
32		1.920(1.887)	0.00814(0.00895)	0.964(0.955)			0.924(0.915)	
	1.122	1.908	0.009	0.958	-0.875	0.483	0.919	[3]

this only for the Ising case $N = 1$, where $\omega = 0.805$. Consider first the function $\bar{g}(\bar{g}_B)$ with the sixth-order strong-coupling expansion (19.10) (whose $\bar{g}_B$-dependence is displayed in Fig. 20.8):

$$\begin{aligned}\bar{g} &= 1.400036164909792 - 2.015076019427151/\bar{g}_B^{\omega} + 2.512390732560552/\bar{g}_B^{2\omega} \\ &- 2.903034628806387/\bar{g}_B^{3\omega} + 3.123423917471507/\bar{g}_B^{4\omega} - 3.108796470872297/\bar{g}_B^{5\omega} \\ &+ 2.844130229268904/\bar{g}_B^{6\omega} - 2.38207097645026/\bar{g}_B^{7\omega}. \end{aligned} \tag{20.29}$$

For $\bar{g}_B \to \infty$, this converges to the fixed point $\bar{g}^* = 1.400036164909792$, the critical coupling constant. The important observation is that by changing variables to $x = x(\bar{g}_B)$ defined by

$$\bar{g}_B \equiv (1-x)/x^{1/\omega}, \tag{20.30}$$

and re-expanding up to the order x^6, we obtain a new modified strong-coupling expansion

$$\begin{aligned}\bar{g}(x) &= 1.400036164909792 - 2.015076019427151x + 0.890254536921696x^2 \\ &- 0.322063465947966x^3 + 0.02243448556302718x^4 + 0.02753503840016558x^5 \\ &+ 0.004440133592881424x^6 - 0.005052466607713413x^7. \end{aligned} \tag{20.31}$$

Numerically, this happens to converge for *all* $\bar{g}_B \in (0, \infty)$ where $x \in (1, 0)$. Indeed, when plotting this function in Fig. 20.8, it falls right on top of the previously calculated curve representing the full variational expression (19.6). To verify the convergence for small couplings,

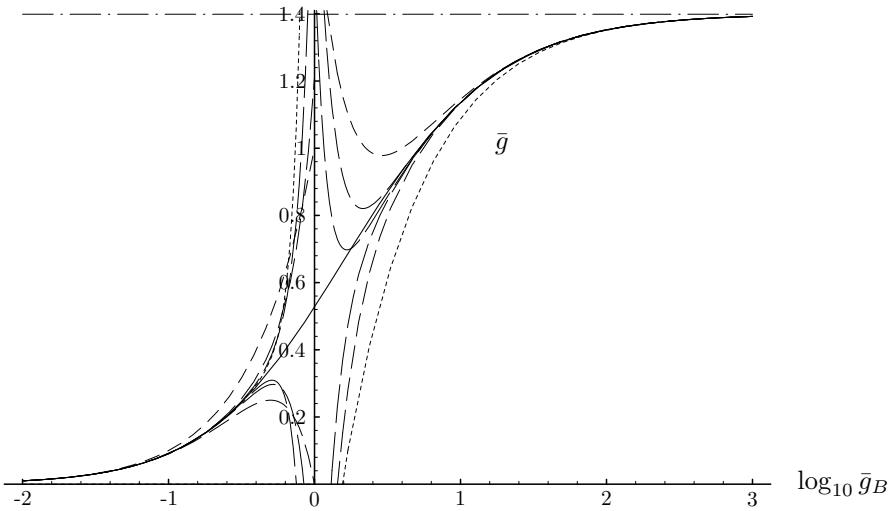

FIGURE 20.8 Logarithmic plot of variational perturbation result for expansion (20.15) of renormalized coupling constant $\bar{g}(\bar{g}_B)$ with $N = 1$ as a function of the bare coupling constant $\bar{g}_B$. The small-$\bar{g}_B$ regime shows truncated divergent perturbation expansions; the large-$\bar{g}_B$ regime shows the truncated strong-coupling expansions. Dash lengths increase with orders. The convergent re-expanded strong-coupling series (20.31) falls on top of the full curve.

we insert $x = 1$ corresponding to $\bar{g}_B = 0$ and obtain 0.0025, which misses only slightly the free-field value 0.

Similarly we obtain a strong-coupling expansion of the critical exponent $\nu(\bar{g}_B)$. In accordance with the above determination of ν from a resummation of the series for the inverse $\nu^{-1}(\bar{g}_B) = 2 - \eta_m(\bar{g}_B)$, we first derive the strong-coupling expansion for the inverse, and invert the resulting power series. The result is

$$\begin{aligned}\nu(\bar{g}_B) &= 0.6264612502473953 - 0.2094930499887895/\bar{g}_B^{\omega} + 0.3174116223980956/\bar{g}_B^{2\omega} \\ &- 0.4674929704457459/\bar{g}_B^{3\omega} + 0.6755577434122434/\bar{g}_B^{4\omega} - 0.961768075384486/\bar{g}_B^{5\omega} \\ &+ 1.35507538545696/\bar{g}_B^{6\omega}. \end{aligned} \tag{20.32}$$

Changing again to the variable $x = x(\bar{g}_B)$, and re-expanding up to the order x^6, we obtain the convergent series

$$\begin{aligned}\nu(x) &= 0.6264612502473953 - 0.2094930499887895x + 0.1487697171571201x^2 \\ &- 0.1086595778647923x^3 + 0.07115354531150436x^4 - 0.04710070728711805x^5 \\ &+ 0.0316053426101743x^6. \end{aligned} \tag{20.33}$$

A plot of this expansion for ν in Fig. 20.9 is again indistinguishable from the full variational perturbation curve for all $\bar{g}_B$. At $x = 1$ corresponding to $\bar{g}_B = 0$, this series gives now 0.5127, which is only about 2% larger than the free-field value 1/2.

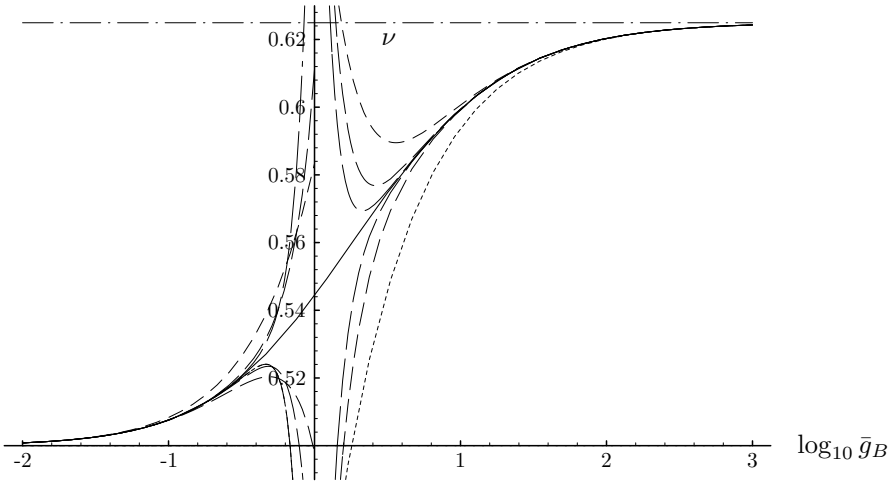

FIGURE 20.9 Logarithmic plot of variational perturbation result for exponent $\nu(\bar{g}_B) = 1/[2-\eta_m(\bar{g}_B)]$ obtained from expansion (20.18) with $N = 1$, and of the convergent re-expanded strong-coupling series (20.35), as a function of the bare coupling constant $\bar{g}_B$. The various dashed curves are explained in Fig. 20.8.

By inverting the series (20.31), we find x as a function of the deviation $\Delta\bar{g} \equiv \bar{g} - \bar{g}^*$ of the renormalized coupling from its strong-coupling value $\bar{g}^*$:

$$\begin{aligned}x(\bar{g}) &= -0.4962591933798516\Delta\bar{g} + 0.1088027548080915\Delta\bar{g}^2 - 0.02817579418977608\Delta\bar{g} \\ &+ 0.005412315522686147\Delta\bar{g}^4 + 0.0000584544818720259 8\Delta\bar{g}^5 \\ &- 0.0006265703321966366\Delta\bar{g}^6 + 0.0002698406382563225\Delta\bar{g}^7. \end{aligned} \tag{20.34}$$

After inserting this into (20.33), we obtain the critical exponent ν as a power series in $\Delta\bar{g}$:

$$\begin{aligned}\nu(\bar{g}) &= 0.6264612502473953 + 0.1039628520061216\Delta\bar{g} + 0.01384457142352891\Delta\bar{g}^2 \\ &+ 0.003117046054051534\Delta\bar{g}^3 + 0.0003684746290205897\Delta\bar{g}^4 \\ &+ 8.64736629778199 \times 10^{-5}\Delta\bar{g}^5 - 7.632599338747235 \times 10^{-6}\Delta\bar{g}^6. \end{aligned} \tag{20.35}$$

In the weak-coupling limit, this is equal to 0.50039 rather than the exact 1/2.

We now turn to $\gamma(\bar{g}_B)$, for which the initial strong-coupling expansion (19.10) reads

$$\begin{aligned}\gamma(\bar{g}_B) &= 1.400036164909792 - 2.015076019427151/\bar{g}_B^{\omega} + 2.512390732560552/\bar{g}_B^{2\omega} \\ &- 2.903034628806387/\bar{g}_B^{3\omega} + 3.123423917471507/\bar{g}_B^{4\omega} - 3.108796470872297/\bar{g}_B^{5\omega} \\ &+ 2.844130229268904/\bar{g}_B^{6\omega} - 2.38207097645026/\bar{g}_B^{6\omega}, \end{aligned} \tag{20.36}$$

which goes over into the following convergent new strong-coupling expansions in the variables x and $\Delta\bar{g}$:

$$\begin{aligned}\gamma(x) &= 1.234453309456454 - 0.3495068067938822x + 0.1754449364006056x^2 \\ &- 0.07496457184890283x^3 + 0.01553288625746019x^4 \\ &- 0.0007559094604789874x^5 - 0.0000549035980521583 9x^6, \qquad (20.37)\\ \gamma(\bar{g}) &= 1.234453309456454 + 0.1734459660202996\Delta\bar{g} + 0.005180080229495593\Delta\bar{g}^2 \\ &+ 0.00006337529084873493\Delta\bar{g}^3 + 7.604216767658758\cdot 10^{-6}\Delta\bar{g}^4 \\ &+ 0.0000397028511191 4907\Delta\bar{g}^5 - 0.0000659750121782 0878\Delta\bar{g}^6. \qquad (20.38)\end{aligned}$$

Combining these expansions with (20.32), (20.33), and (20.35), we derive from the scaling relation $\eta = 2 - \gamma/\nu$ the corresponding expansions for η:

$$\begin{aligned}\eta(\bar{g}_B) &= 0.02948177725444778 - 0.101048653404458/\bar{g}_B^{\omega} + 0.2354470919307273/\bar{g}_B^{2\omega} \\ &- 0.452249390223013/\bar{g}_B^{3\omega} + 0.7620101849621524/\bar{g}_B^{4\omega} \\ &- 1.160617256113553/\bar{g}_B^{5\omega} + 1.627651002530155/\bar{g}_B^{6\omega}, \qquad (20.39)\\ \eta(x) &= 0.02948177725444778 - 0.101048653404458x + 0.1541029259401388x^2 \\ &- 0.1465926820210476x^3 + 0.0958727624055483x^4 \\ &- 0.04186840682453081x^5 + 0.01220597704767396x^6, \qquad (20.40)\\ \eta(\bar{g}) &= 0.02948177725444778 + 0.05014632323061653\Delta\bar{g} + 0.02695704683941055\Delta\bar{g}^2 \\ &+ 0.004121619548050133\Delta\bar{g}^3 - 0.0003823552182275 9\Delta\bar{g}^4 \\ &+ 0.0000173670055184726 2\Delta\bar{g}^5 + 0.0000435880986255714\Delta\bar{g}^6. \qquad (20.41)\end{aligned}$$

The weak-coupling limits of these expansions are $\gamma(x = 1) = 1.00015$, $\gamma(\bar{g}_B = 0) = 1.00092$ rather than the exact 1; and $\eta(x = 1) = 0.0025$, $\eta(\bar{g}_B = 0) = 0.00043$ rather than the exact 0. The expansions for $\eta(x)$ converge rather slowly, so it is preferable to do calculations involving η by replacing it by $\eta = 2 - \gamma/\nu$ and using the expansions for γ and ν without re-expanding the ratio γ/ν. Then the plots of the convergent expansion for $\gamma(x)$ and of $\eta(x)$ are found once more to be very close to the plots of the corresponding full sixth-order approximations, as shown in Fig. 20.10.

It is now easy to give convergent expansions for the full m_B dependence of the renormalization factors. From (20.8) we see that

$$\frac{m^2}{m_B^2} = \exp\left[-\int_0^{\bar{g}_B}\frac{d\bar{g}'_B}{\bar{g}'_B}\eta_m(\bar{g}'_B)\right] = \frac{m^2}{g_B^2}\exp\left[-\int_x^1\frac{dx'}{x'}\frac{\eta_m(x')}{f(x')}\right], \qquad (20.42)$$

$$\frac{\phi^2}{\phi_B^2} = \exp\left[\int_0^{\bar{g}_B}\frac{d\bar{g}'_B}{\bar{g}'_B}\eta(\bar{g}'_B)\right] = \exp\left[\int_x^1\frac{dx'}{x'}\frac{\eta(x')}{f(x')}\right], \qquad (20.43)$$

where we have introduced the function

$$f(x) \equiv -\frac{d\log x}{d\log\bar{g}_B} = \omega\frac{1-x}{1-(1-\omega)x}. \qquad (20.44)$$

After isolating the logarithmic divergence of the integrals at $x = 0$, these can be rewritten as

$$\frac{m^2}{m_B^2} = x^{\eta_m/\omega}e^{-I_m(x)}, \qquad \frac{\phi^2}{\phi_B^2} = x^{-\eta/\omega}e^{I(x)}, \qquad (20.45)$$

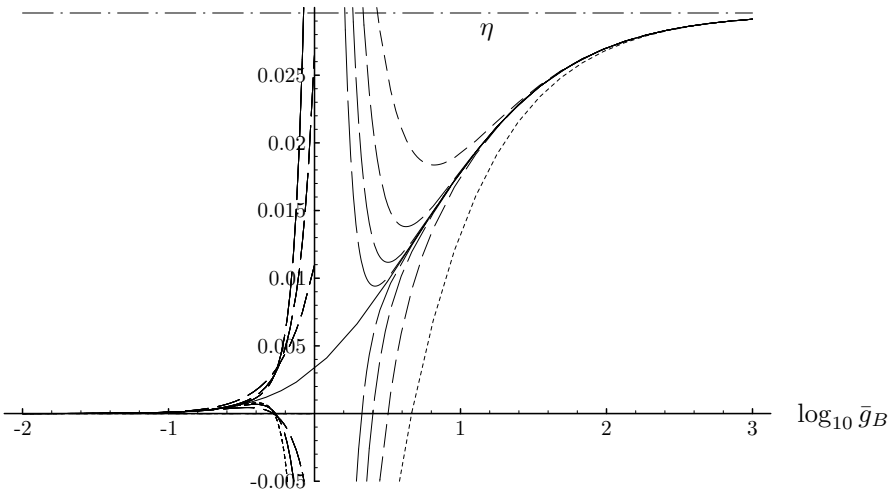

FIGURE 20.10 Logarithmic plot of variational perturbation result for expansion (20.17) of exponent $\eta(\bar{g}_B)$ with $N = 1$, and of the convergent re-expanded strong-coupling series (20.40) as a function of the bare coupling constant $\bar{g}_B$. The various dashed curves are explained in Fig. 20.8.

where $I(x)$ and $I_m(x)$ are the subtracted finite integrals

$$I_m(x) = \int_x^1 \frac{dx'}{x'} \left[\frac{\eta_m(x')}{f(x')} - \frac{\eta_m}{\omega} \right], \qquad I(x) = \int_x^1 \frac{dx'}{x'} \left[\frac{\eta(x')}{f(x')} - \frac{\eta}{\omega} \right]. \tag{20.46}$$

The integral $I_m(x)$ can readily be performed using a power series for $\eta_m(x)$ obtained from (20.33) via $\eta_m(x) = 2 - \nu^{-1}(x)$. The result is

$$\begin{aligned} I_m(x) &= 0.3023858220717581 - 0.3374211153180052x + 0.05257791758557147x^2 \\ &- 0.02006073290035280x^3 + 0.002720917209250741x^4 - 0.0001454953425150762x^5 \\ &- 0.00005731330570724153x^6. \end{aligned} \tag{20.47}$$

By combining the second equation in (20.45) with (20.30), rewritten as

$$\frac{m^2}{g_B^2} = x^{2/\omega}(1-x)^{-2}, \tag{20.48}$$

we find

$$\frac{m_B^2}{g_B^2} = x^{1/\nu\omega}(1-x)^{-2} e^{I_m(x)}. \tag{20.49}$$

In the weak-coupling limit $x \to 1$, the integral vanishes and the renormalized mass approaches the bare mass. In the strong-coupling limit $x \to 0$, on the other hand, $I_m(x)$ becomes a constant and we obtain once more the scaling relation $m \propto m_B^{2\nu}$. To study the crossover from the weak to the strong-coupling behavior exhibiting the critical behavior, we define a temperature interval ΔT_F within which fluctuations are important, and set

$$\frac{m_B^2}{g_B^2} \equiv \frac{T - T_c}{\Delta T_F} \equiv \tau_{\rm red}. \tag{20.50}$$

A doubly logarithmic plot of the inverse square coherence length $\xi^{-2} \propto m^2/g_B$ in Fig. 20.11 shows how the slope changes from the free-field value 1 at large temperatures to 2ν near the critical temperature T_c.

Let us compare the fluctuation interval ΔT_F with the characteristic Ginzburg temperature interval $\Delta T_G = T_c^{\rm MF}\tau_G$ determined by Eq. (1.106). Recalling the normalization of the coupling strength in Eq. (20.1), we identify the parameter K in Eq. (1.105) as

$$K = 2^{D/2-1}\frac{48\pi}{N+8}\frac{g_B}{6}, \tag{20.51}$$

having inserted $A_1 = 1$ and $a_2 = 1$, corresponding to $A_2 = m_B^2 = \tau = (T/T_c^{\rm MF} - 1)$ in (1.83). Using the cell size parameter $l = 1$ in (1.104), we insert the Yukawa potential at the orign $v_1^3(\mathbf{0}) \approx 0.1710$ from Table 1.1 , and obtain

$$\tau_G = \left[Kv_1^3(\mathbf{0})\right]^2 g_B^2 \approx 0.456\, g_B^2. \tag{20.52}$$

Thus we have

$$\Delta T_F \approx 2.2\Delta T_G, \tag{20.53}$$

implying that the deviations from the mean-field behavior in Fig. 20.11 are in good agreement with Ginzburg's criterion.

For higher O(N) symmetries, the same type of agreement would be found for the onset of directional fluctuations by applying Kleinert's criterion of Subsection 1.4.3. Indeed, the denominator $(N + 8)$ in Eq. (20.51) is canceled roughly by the factor N in formula (1.115) for Kleinert's temperature interval ΔT_K, such that the fluctuation temperature interval ΔT_F is of the same order of magnitude as $\Delta T_K = T_c^{\rm MF}\tau_K$.

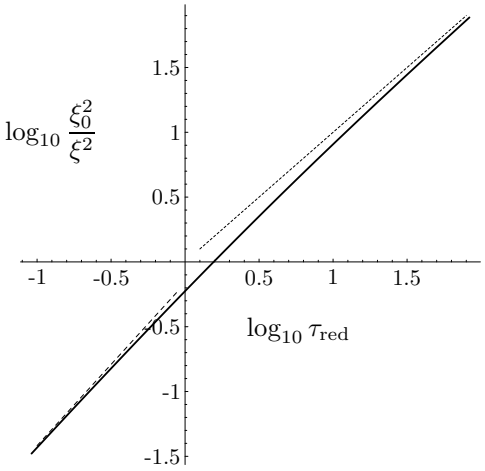

FIGURE 20.11 Doubly logarithmic plot of inverse square coherence length ξ^{-2} in arbitrary units against the reduced temperature $\tau_{\rm red} \equiv (T - T_c)/\Delta T_F$, where ΔT_F is the fluctuation temperature interval (20.50), closely related to Ginzburg's temperature by Eq. (20.53), where the theory crosses over from free field to critical behavior. The dotted line shows the free-field limit with unit slope, the dashed line the strong-coupling limit with slope $2\nu \approx 1.252$.

Finally, we use the series (20.31) for $\bar{g}(x)$ to calculate the β-function which plays an important role in the renormalization group approach to scaling (in contrast to our explicit theory). By definition, we obtain it as a function of x from the logarithmic derivative of $\bar{g}(\bar{g}_B)$ [compare (20.3)]

$$\beta(x) = -\bar{g}_B\frac{d\bar{g}}{d\bar{g}_B} = f(x)\,\bar{g}'(x), \tag{20.54}$$

with $f(x)$ from (20.44), the result being

$$\begin{aligned}\beta(x) &= -1.622136195638856x + 2.73912944193321x^2 - 1.676962833531292x^3 \\ &+ 0.5230145612386834x^4 + 0.1405773254892622x^5 - 0.06197010583664305x^6 \\ &- 0.06200066522622774x^7. \end{aligned} \tag{20.55}$$

The convergence of this strong-coupling expansion is seen by going to the weak-coupling limit $x = 1$ corresponding to $\bar{g}_B = 0$ where we find $\beta(1) = -0.0046$ rather than the exact value 0. Expressing x as a function of $\Delta\bar{g}$ via (20.34), we obtain

$$\begin{aligned}\beta(\bar{g}) &= 0.805\Delta\bar{g} + 0.4980812505494033\Delta\bar{g}^2 - 0.04513957559397346\Delta\bar{g}^3 \\ &- 0.002836436593862963\Delta\bar{g}^4 + 0.0008110679470657 38\Delta\bar{g}^5 \\ &+ 0.002150487674009535\Delta\bar{g}^6 - 0.002024061592617085\Delta\bar{g}^7, \end{aligned} \tag{20.56}$$

which is plotted in Fig. 20.12.

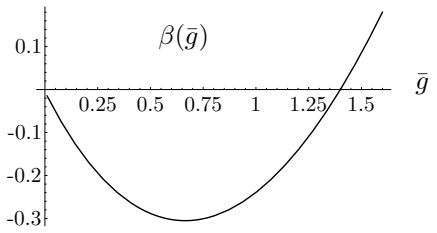

FIGURE 20.12 Plot of convergent strong-coupling expansion (20.56) for the beta function $\beta(\bar{g})$. The slope at the zero is the critical exponent $\omega = 0.805$. Note that the function converges well also at weak couplings. The curve misses the coordinate origin only by a very small amount.

From this we can derive the function $\omega(\bar{g})$ by a simple derivative with respect to $\bar{g}$:

$$\begin{aligned}\omega(\bar{g}) = \beta'(\bar{g}) &= 0.805 + 0.996162501098807\Delta\bar{g} - 0.1354187267819204\Delta\bar{g}^2 \\ &- 0.01134574637545185\Delta\bar{g}^3 + 0.004055339735328691\Delta\bar{g}^4 \\ &+ 0.01290292604405721\Delta\bar{g}^5 - 0.01416843114831959\Delta\bar{g}^6. \end{aligned} \tag{20.57}$$

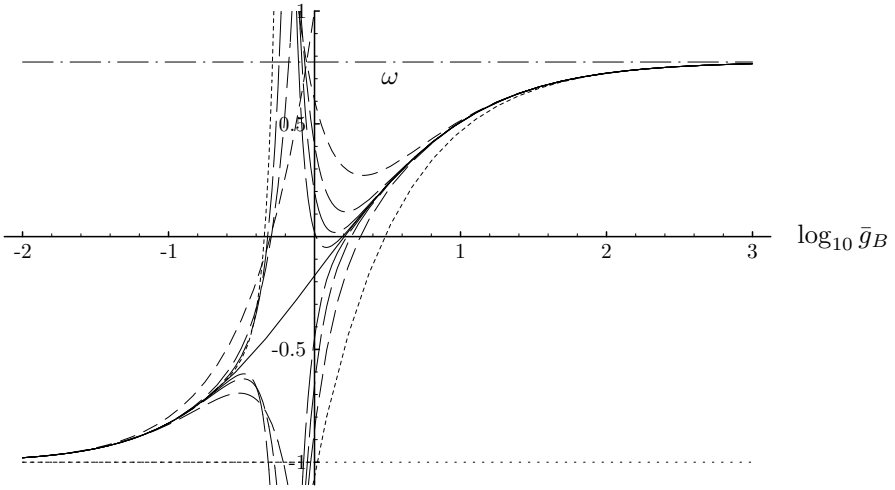

FIGURE 20.13 Logarithmic plot of variational perturbation result for expansion (20.16) with $N = 1$, and of the convergent re-expanded strong-coupling series (20.57) for exponent $\omega(\bar{g}_B)$, as a function of the bare coupling constant $\bar{g}_B$. The various dashed curves are explained in Fig. 20.8.

At $\bar{g} = \bar{g}^*$, the function $\omega(\bar{g}_B)$ has the value 0.805 as it should. In the weak-coupling limit $\bar{g}_B = 0$, it is equal to $-.984$, very close to the exact value -1. The full plot is shown in Fig. 20.13.

As a check for the consistent accuracy of our expansion procedures, we calculate ω once more from

$$\omega = -\frac{\bar{g}_B}{\beta(\bar{g})}\frac{d\beta(\bar{g})}{d\bar{g}_B} = f(x)\frac{x}{\beta(x)}\beta'(x). \tag{20.58}$$

After expressing x in terms of $\Delta\bar{g}$ we obtain a series with coefficients very close to those in (20.57), with only a slightly worse weak-coupling limit -1.08 rather than -1.

20.3 Improving the Graphical Extrapolation of Critical Exponents

In the last section, the critical exponents were obtained by extrapolating the approximations of order $2, 3, 4, 5$, and 6 to order $L \to \infty$ using the theoretically calculated large-L behavior const$+e^{-cL^{1-\omega}}$. The plots showed how the exponents approach their limiting values as functions of N. Exploiting this knowledge of the analytic form of the approach to infinite L, we plot the approximate exponents once more against the variable $x(L) = e^{-cL^{1-\omega}}$ rather than L [20], as done in Section 19.7. The parameter c is determined by varying it until the points merge approximately into a straight line for large L. Its intercept with the vertical axis yields the desired extrapolated critical exponent. The plots displayed in Figs. 20.14–20.17 show that variational strong-coupling theory provides us with a powerful tool for deriving the correct strong-coupling behavior and critical exponents of ϕ^4-theories in three dimensions.

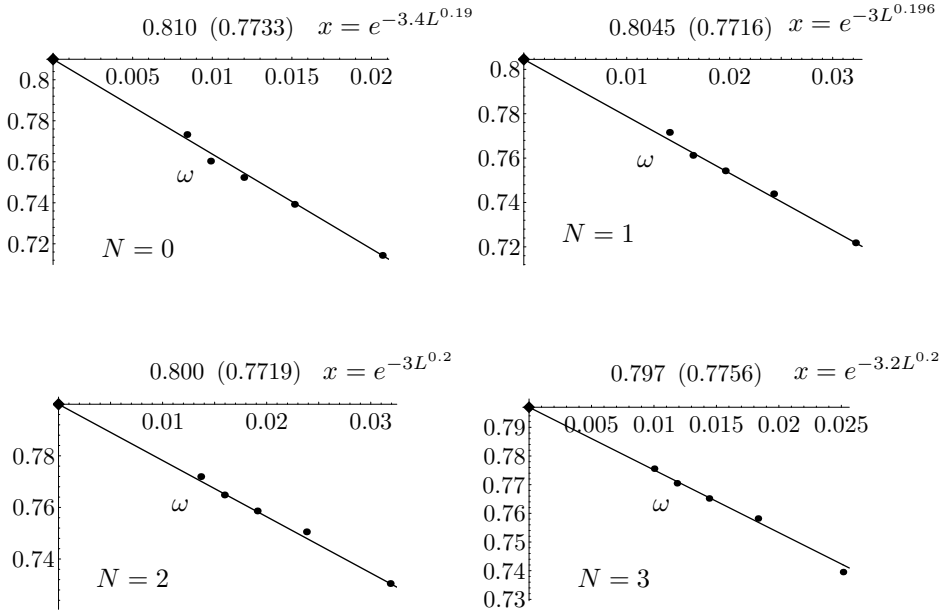

FIGURE 20.14 Behavior of strong-coupling values of the critical exponent of approach to scaling ω with increasing orders $L = 2, 3, 4, 5, 6$ in variational perturbation theory for O(N)-symmetric theories with $N =$ 0, 1, 2, 3, ... The plot is against $x(L) = e^{-cL^{1-\omega}}$ with c chosen such that the points merge into a straight line. The numbers N correspond to different universality classes ($N = 0, 1, 2, 3$ for dilute polymer solutions, Ising magnets, superfluid helium, and the classical Heisenberg model). The numbers on top display the limiting value at the intercept, as well as the last calculated approximation ω_6 in parentheses (see Table 20.1 on page 375).

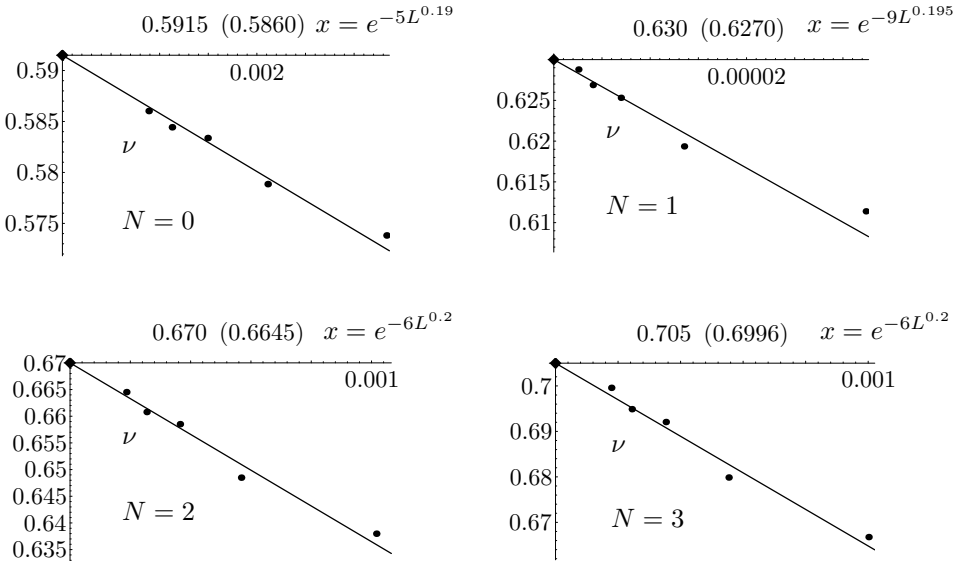

FIGURE 20.15 Plot analogous to Fig. 20.14 of critical exponents ν, for increasing orders $L = 2, 3, 4, 5, 6$ in variational perturbation theory, illustrating the extrapolation procedure to $N \to \infty$ at the intercept with the vertical axis, for $N = 0,\ 1,\ 2,\ 3$. The numbers on top display the limiting value at the intercept, as well as the last calculated approximation ν_6 in parentheses (see Table 20.1 on page 375).

20.4 Seven-Loop Results for $N = 0, 1, 2,$ and 3

For O(N)-symmetric theories with $N = 0, 1, 2, 3$, the power series expansions (20.12) and (20.13) have recently been calculated up to seven loops [12]. The results are [13]

$$f_7^{\eta} = \left\{ \begin{array}{l} 0.001901867 \\ 0.001697694 \\ 0.001395129 \\ 0.001111499 \end{array} \right\} \bar{g}^7, \qquad f_7^{\eta_m} = \left\{ \begin{array}{l} 0.097383003 \\ 0.091551786 \\ 0.079018231 \\ 0.065974801 \end{array} \right\} \bar{g}^7 \qquad \text{for} \qquad \left\{ \begin{array}{l} N = 0 \\ N = 1 \\ N = 2 \\ N = 3 \end{array} \right\}. \tag{20.59}$$

In the expansions (20.17), (20.18), and (20.19) of η, η_m, and γ in powers of the bare couplings $\bar{g}_B$, these add the terms

$$f_7^{\eta} = \left\{ \begin{array}{l} -0.216423937 \\ -0.239546791 \\ -0.241424764 \\ -0.233364541 \end{array} \right\} \bar{g}_B^7, \ f_7^{\eta_m} = \left\{ \begin{array}{l} 6.099829565 \\ 7.048219834 \\ 7.378080984 \\ 7.380848508 \end{array} \right\} \bar{g}_B^7, \ f_7^{\gamma} = \left\{ \begin{array}{l} 2.504064047 \\ 2.650615568 \\ 2.570336644 \\ 2.401546939 \end{array} \right\} \bar{g}_B^7, \tag{20.60}$$

respectively.

We now calculate the strong-coupling limit of the seven-loop power series expansions (20.18) for η_m, extended by $f_7^{\eta_m}$. Using formula (19.16) with $q = 2/\omega$ and ω from Table 20.1 on page 375, we obtain the limiting values for $\nu = 1/(2 - \eta_m)$ shown in Fig. 20.18. They lead to the ν-values $\nu_7 = \{0.5886, 0.6311, 0.6713, 0.7072\}$, the entries in this vector referring to

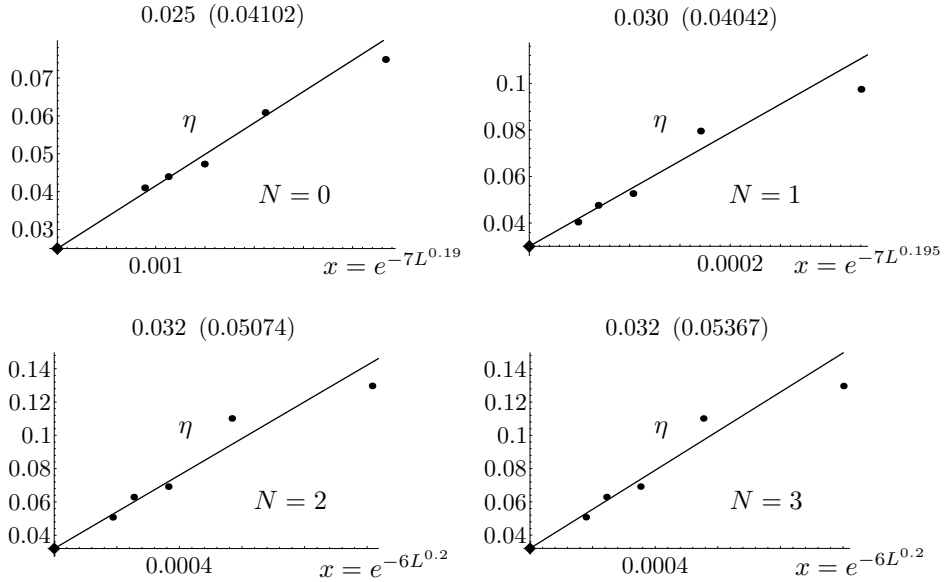

FIGURE 20.16 Plot analogous to Figs. 20.14 and 20.15 of critical exponents η, for increasing orders $L = 2, 3, 4, 5, 6$ in variational perturbation theory, illustrating the extrapolation procedure to $N \to \infty$ at the intercept with the vertical axis, for $N = 0,\ 1,\ 2,\ 3$. The approximations η_L are obtained from γ_L via the scaling relation $\eta_L = 2 - \gamma_L/\nu$. The numbers on top display the limiting value at the intercept, as well as the last calculated approximation η_6 in parentheses (see Table 20.1 on page 375).

$N = 0, 1, 2, 3$. These results are derived using the six-loop ω-values listed in the last column of Table 20.1 on page 375:

$$\omega_6 = \left\{ \begin{array}{l} 0.810 \\ 0.805 \\ 0.797 \\ 0.790 \end{array} \right\} \quad \text{for} \quad \left\{ \begin{array}{l} n = 0 \\ n = 1 \\ n = 2 \\ n = 3 \end{array} \right\}. \tag{20.61}$$

It is useful to study the dependence of the extrapolation on ω. The result is

$$\nu_7 = \left\{ \begin{array}{l} 0.5883 + 0.0417 \times (\omega - 0.810) \\ 0.6305 + 0.0400 \times (\omega - 0.805) \\ 0.6710 + 0.0553 \times (\omega - 0.800) \\ 0.7075 + 0.1891 \times (\omega - 0.797) \end{array} \right\} \quad \text{for} \quad \left\{ \begin{array}{l} N = 0 \\ N = 1 \\ N = 2 \\ N = 3 \end{array} \right\}. \tag{20.62}$$

We extrapolate our results to $L = \infty$ by plotting the data against the variables $x(L) = e^{-cL^{1-\omega}}$, as in Section 20.3. However, since we are now in the possession of an even number of approximants $\nu_2, \ldots, \nu_7$, we may account for the fact that even and odd approximants are obtained differently, the former from extrema, the latter from turning points of the variational expression (19.16). We therefore plot even and odd approximants separately against $x(L)$, determining the unknown constants c by fitting to each set of points a slightly curved parabola and making them intersect the vertical axis at the same point. This yields the extrapolated critical exponent listed on top of each figure (together with the seventh-order value in parentheses, and the optimal parameter c).

For the critical exponent η we cannot use the same extrapolation procedure since the expansion (20.17) starts out with $\bar{g}_0^2$, so that there exists only an odd number of approximants η_L. We therefore use two alternative extrapolation procedures. In the first we connect the even approximants η_2 and η_4 by a straight line and the odd ones η_3, η_5, η_7 by a slightly curved

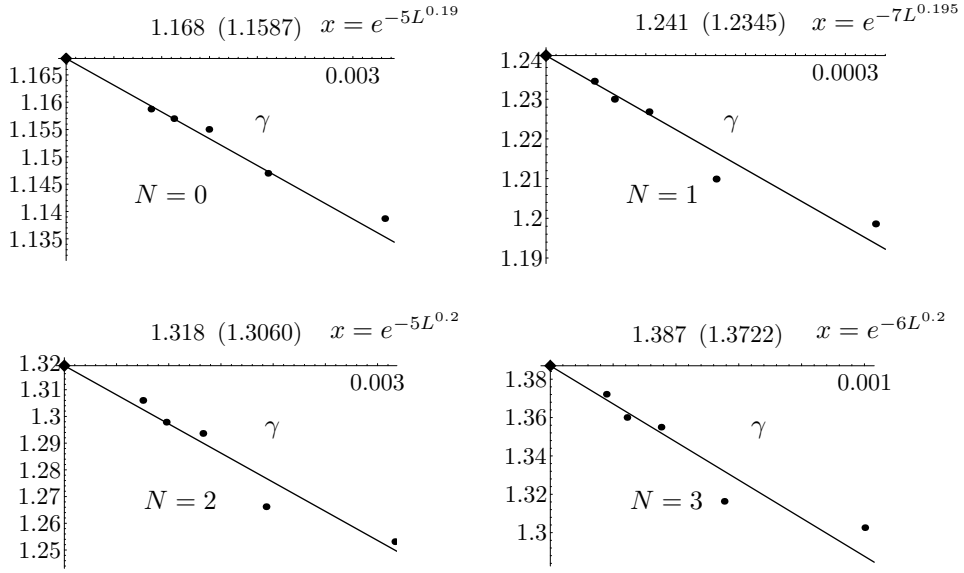

FIGURE 20.17 Plot analogous to Figs. 20.14, 20.15, and 20.16 of critical exponents γ, for increasing $L = 2, 3, 4, 5, 6$ in variational perturbation theory, illustrating the extrapolation procedure to $N \to \infty$ at the intercept with the vertical axis, for $N = 0,\ 1,\ 2,\ 3$. The numbers on top display the limiting value at the intercept, as well as the last calculated approximation γ_6 in parentheses (see Table 20.1 on page 375).

parabola, allowing for smooth approach to the asymptotic behavior of the three available odd approximations. Then we vary c until there is an intersection at $x = 0$. This yields the critical exponents η shown in Fig. 20.19.

Allowing for the inaccurate knowledge of ω, the results may be stated as

$$\eta_7 = \left\{ \begin{array}{l} 0.03215 + 0.1327 \times (\omega - 0.810) \\ 0.03572 + 0.0864 \times (\omega - 0.805) \\ 0.03642 + 0.0655 \times (\omega - 0.800) \\ 0.03549 + 0.0320 \times (\omega - 0.797) \end{array} \right\} \quad \text{for} \quad \left\{ \begin{array}{l} N = 0 \\ N = 1 \\ N = 2 \\ N = 3 \end{array} \right\}, \tag{20.63}$$

Alternatively, we connect the last odd approximants η_5 and η_7 also by a straight line and choose c to make the lines intersect at $x = 0$. This yields the exponents

$$\eta_7 = \left\{ \begin{array}{l} 0.03010 + 0.08760 \times (\omega - 0.810) \\ 0.03370 + 0.03816 \times (\omega - 0.805) \\ 0.03480 + 0.01560 \times (\omega - 0.800) \\ 0.03447 + 0.00588 \times (\omega - 0.797) \end{array} \right\} \quad \text{for} \quad \left\{ \begin{array}{l} N = 0 \\ N = 1 \\ N = 2 \\ N = 3 \end{array} \right\}, \tag{20.64}$$

as shown in Fig. 20.20, the ω dependences being somewhat weaker than in (20.63).

Combining the two results and using the difference to estimate the systematic error of the extrapolation procedure, we obtain for η the values

$$\eta_7 = \left\{ \begin{array}{l} 0.0311 \pm 0.001 \\ 0.0347 \pm 0.001 \\ 0.0356 \pm 0.001 \\ 0.0350 \pm 0.001 \end{array} \right\} \quad \text{for} \quad \left\{ \begin{array}{l} N = 0 \\ N = 1 \\ N = 2 \\ N = 3 \end{array} \right\}, \tag{20.65}$$

whose ω-dependence is the average of that in (20.63) and (20.64).

For our extrapolation procedure, the power series for the critical exponent $\gamma = \nu(2 - \eta)$ are actually better suited than those for η, since they possess three even and three odd

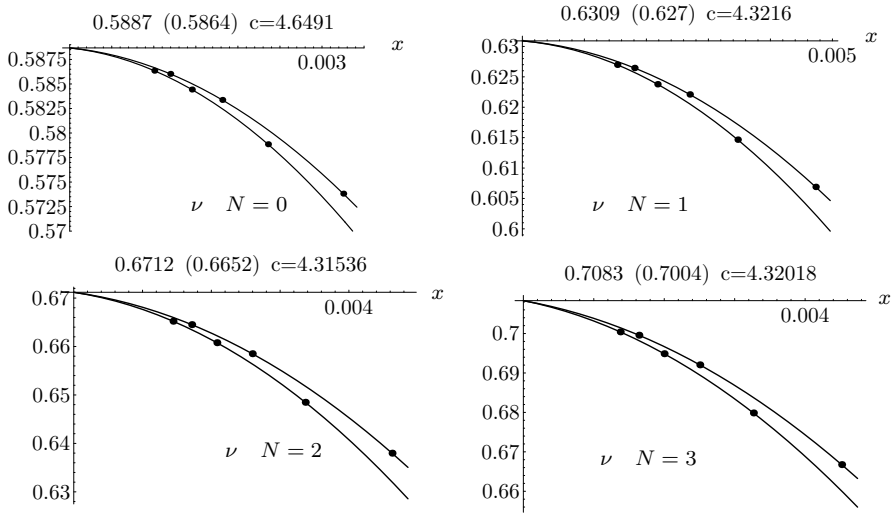

FIGURE 20.18 Strong-coupling values for the critical exponent ν^{-1} obtained from expansion (20.18) via formula (19.16), for increasing orders $L = 2, 3, \ldots, 7$ of the approximation. The exponents are plotted against the variable $x(L) = e^{-cL^{1-\omega}}$ and should lie on a straight line in the limit of large L. Here at finite L, even and odd approximants may be connected by slightly curved parabolas whose common intersection determines the critical exponents for $L = \infty$. More details on the determination of the constant c are given in the text.

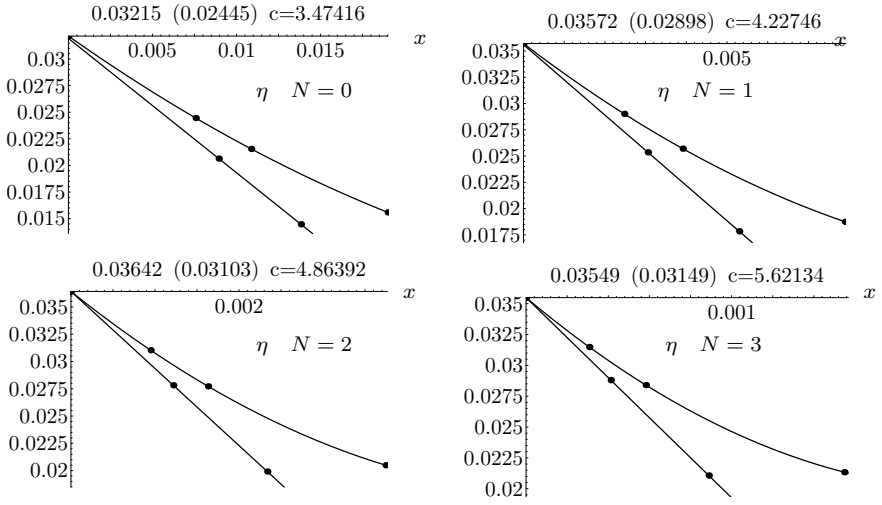

FIGURE 20.19 Strong-coupling values for the critical exponent η obtained from expansion (20.17), extended by f_7^η of Eq. (20.60), via formula (19.16), for increasing orders $L = 3, \ldots, 7$ of the approximation. The exponents are plotted against $x(L) = e^{-cL^{1-\omega}}$. Even approximants are connected by straight line and odd approximants by slightly curved parabolas, whose common intersection determines the critical exponents expected for $L = \infty$.

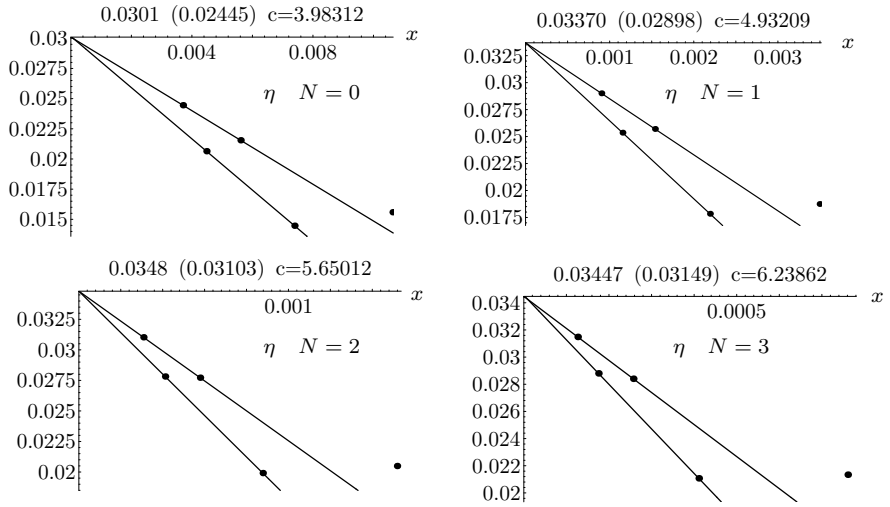

FIGURE 20.20 Plot analogous to Fig. 20.19, but with an extrapolation found from the intersection of the straight lines connecting the last two even and odd approximants. The resulting critical exponents differ only little from those obtained in Fig. 20.19, the differences giving an estimate for the systematic error of our results.

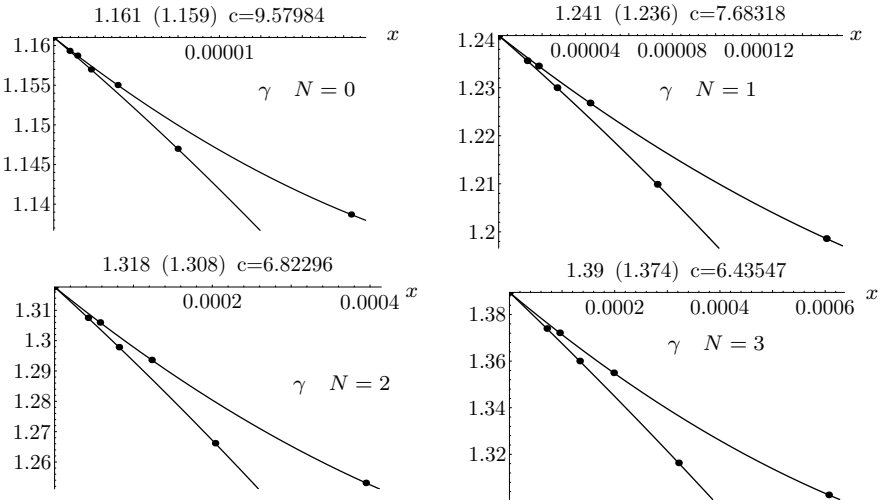

FIGURE 20.21 Strong-coupling values for the critical exponent $\gamma = \nu(2-\eta) = (2-\eta)/(2-\eta_m)$ obtained from a combination of the expansions (20.17) and (20.18), optimizing the associated expression (19.16), for increasing orders $N = 2, 3, \ldots, 7$ of the approximation. The exponents are plotted against the variable $x(L) = e^{-cL^{1-\omega}}$ and should lie on a straight line in the limit of large L. Even and odd approximants are connected by slightly curved parabolas whose common intersection determines the critical exponents expected for $L = \infty$. The determination of the constant c is described in the text.

approximants, just as ν^{-1}. Advantages of this expansion have been observed before in Ref. [4]. The associated plots are shown in Fig. 20.21.

The extrapolated exponents are, including the ω-dependence:

$$\gamma_7 = \left\{ \begin{array}{l} 1.161 - 0.049 \times (\omega - 0.810) \\ 1.241 - 0.063 \times (\omega - 0.805) \\ 1.318 - 0.044 \times (\omega - 0.800) \\ 1.390 - 0.120 \times (\omega - 0.797) \end{array} \right\} \quad \text{for} \quad \left\{ \begin{array}{l} N = 0 \\ N = 1 \\ N = 2 \\ N = 3 \end{array} \right\}. \tag{20.66}$$

Unfortunately, the exponent $\gamma = \nu(2-\eta)$ is not very sensitive to η since this is small compared to 2, so that the extrapolation results (20.63) are more reliable than those obtained from γ via the scaling relation $\eta = 2 - \gamma/\nu$. By combining (20.62) and (20.63), we find from $\gamma = \nu(2-\eta)$:

$$\gamma_7 = \left\{ \begin{array}{l} 1.1589 \\ 1.2403 \\ 1.3187 \\ 1.3932 \end{array} \right\} \quad \text{for} \quad \left\{ \begin{array}{l} N = 0 \\ N = 1 \\ N = 2 \\ N = 3 \end{array} \right\}, \tag{20.67}$$

the difference with respect to (20.66) showing the typical small errors of our approximation.

As mentioned in the beginning, the knowledge of the large-order behavior does not help to improve significantly the accuracy of the approximation. In our theory, the most important information exploited by the resummation procedure is the knowledge of the exponentially fast convergence which leads to a linear behavior of the resummation results of order L in a plot against $x(L) = e^{-cL^{1-\omega}}$. This knowledge, which allows us to extrapolate our approximations for $L = 2, 3, 4, 5, 6, 7$ quite well to infinite order L, seems to be more powerful than the knowledge of the large-order behavior exploited by other authors (quoted in Table 20.1 on page 375).

The complete updated list of exponents is shown in Table 20.2 , which also contains values for the other critical exponents $\alpha = 2 - D\nu$ and $\beta = \nu(D - 2 + \eta)/2$.

20.5 Large-Order Behavior

The new coefficients follow quite closely their theoretically expected large-order limiting behavior derived from instanton calculations, according to which the expansion coefficients with respect to the renormalized coupling $\bar{g}$ should grow for large order k as follows [recall Eq. (16.12)]:

$$f_k^\omega = \gamma_\omega (-\alpha)^k k! k\Gamma(k + \beta_\omega) \left(1 + \frac{c_\beta^{(1)}}{k} + \frac{c_\beta^{(2)}}{k^2} + \dots \right), \tag{20.68}$$

$$f_k^\eta = \gamma_\eta (-\alpha)^k k! k\Gamma(k + \beta_\eta) \left(1 + \frac{c_\eta^{(1)}}{k} + \frac{c_\eta^{(2)}}{k^2} + \dots \right), \tag{20.69}$$

$$f_k^{\bar\eta} = \gamma_{\bar\eta} (-\alpha)^k k! k\Gamma(k + \beta_{\bar\eta}) \left(1 + \frac{c_{\bar\eta}^{(1)}}{k} + \frac{c_{\bar\eta}^{(2)}}{k^2} + \dots \right), \tag{20.70}$$

where $\bar\eta \equiv \eta + \nu^{-1} - 2$. The growth parameter α is proportional to the inverse euclidean action of the classical *instanton* solution $\varphi_c(\mathbf{x})$ to the field equations, and an accurate numerical evaluation yields [15]

$$\alpha = (D-1)\frac{16\pi}{I_4}\frac{1}{N+8} \stackrel{D=3}{=} 0.14777423\frac{9}{N+8}. \tag{20.71}$$

TABLE 20.2 Seven-loop results for critical exponents $N = 0$, 1, 2, 3 from strong-coupling theory, improving the six-loop results of Table 20.1 on page 375. The ω-values in the last column are six-loops results, the references [14] and [12] seven-loop results. To facilitate the comparison with the earlier results in Table 20.1 we have repeated the former six-loop entries.

N	g_c	$\gamma(\gamma_6)$	$\eta(\eta_6)$	$\nu(\nu_6)$	α	β	ω (ω_6)	
0		1.161(1.159)	0.0311±0.001	0.5886(0.5864)	0.234		0.810(0.773)	
	1.413±0.006	1.160±0.002	0.0284±0.0025	0.5882±0.0011	0.235±0.003	0.3025±0.0008	0.812±0.016	[14]
	1.39	1.1569±0.0004	0.0297±0.0009	0.5872±0.0004	0.2384±0.0012			[12]
	1.402	1.160	0.034	0.589	0.231	0.305		[3]
	1.421±0.004	1.161±0.003	0.026±0.026	0.588±0.001	0.236±0.004	0.302±0.004	0.794 ± 0.06	[2]
	1.421 ± 0.008	1.1615 ± 0.002	0.027 ± 0.004	0.5880±0.0015		0.3020±0.0015	0.80 ± 0.04	[9]
		1.160 ± 0.004	0.031 ± 0.003	0.5885±0.0025		0.3025±0.0025	0.82 ± 0.04	[11]
1		1.241(1.236)	0.0347±0.001	0.6310(0.6270)	0.107		0.805(0.772)	
	1.411±0.004	1.240±0.001	0.0335±0.0025	0.6304±0.0013	0.109±0.004	0.3258±0.0014	0.799±0.011	[14]
	1.40	1.2378±0.0006	0.0355±0.0009	0.6301±0.0005	0.1097±0.0012			[12]
	1.419	1.239	0.038	0.631	0.107	0.327	0.781	[3]
	1.416±0.0015	1.241±0.004	0.031±0.011	0.630±0.002	0.110 ± 0.008	0.324 ± 0.06	0.788 ± 0.003	[2]
	1.416±0.004	1.2410±0.0020	0.031±0.004	0.6300±0.0015		0.3250±0.0015	0.79±0.03	[9]
			0.035 ± 0.002	0.628±0.001			0.80 ± 0.02	[10]
		1.1239 ± 0.004	0.037 ± 0.003	0.6305±0.0025		0.3265±0.0025	0.81 ± 0.04	[11]
2		1.318(1.306)	0.0356 ± 0.001	0.6713(0.6652)	-0.0129		0.800(0.772)	
	1.403±0.003	1.317±0.002	0.0354±0.0025	0.6703±0.0013	-0.011±0.004	0.3470±0.0014	0.789±0.011	[14]
	1.40	1.3178±0.001	0.0377±0.0006	0.6715±0.0007	-0.0145±0.0021			[12]
	1.408	1.315	0.039	0.670	-0.010	0.348	0.780	[3]
	1.406±0.005	1.316±0.009	0.032±0.015	0.669±0.003	-0.007±0.009	0.346±0.009	0.78 ± 0.01	[2]
	1.406±0.004	1.3160±0.0025	0.033±0.004	0.6690±0.0020		0.3455±0.002	0.78±0.025	[9]
			0.037 ± 0.002	0.665±0.001			0.79 ± 0.02	[10]
		1.315 ± 0.007	0.040 ± 0.003	0.671±0.005		0.3485±0.0035	0.80 ± 0.04	[11]
3		1.390(1.374)	0.0350 ± 0.0005	0.7072(0.7004)	-0.122		0.797(0.776)	
	1.391±0.004	1.390±0.005	0.0355±0.0025	0.7073±0.0030	-0.122±0.009	0.3662±0.0025	0.782±0.0013	[14]
	1.39	1.3926±0.001	0.0374±0.0004	0.7096±0.0008	-0.1288±0.0024			[12]
	1.392	1.386	0.038	0.706	-0.117	0.366	0.780	[3]
	1.392±0.009	1.390±0.01	0.031±0.022	0.705±0.005	-0.115±0.015	0.362	0.78 ± 0.02	[2]
	1.391 ±0.004	1.386±0.004	0.033±0.004	0.705±0.003		0.3645±0.0025	0.78 ± 0.02	[9]
			0.037 ± 0.002	0.79±0.02			0.79 ± 0.02	[10]
		1.390 ± 0.010	0.040 ± 0.003	0.710±0.007		0.368±0.004	0.79 ± 0.04	[11]

The quantity I_4 denotes the integral

$$I_4 = \int d^D x [\varphi_c(\mathbf{x})]^4. \tag{20.72}$$

Its numerical values in two and three dimensions D are listed in Table 20.3 .

TABLE 20.3 Fluctuation determinants and integrals over extremal field solution.

D	D_L	D_T	I_1	I_4	I_6	H_3
3	10.544 ± 0.004	1.4571± .0001	31.691522	75.589005	659.868352	13.563312
2	135.3 ± 0.1	1.465± 0.001	15.10965	23.40179	71.08023	9.99118

The growth parameters $\beta_\omega, \beta_\eta, \beta_{\bar\eta}$, are related to the number of zero-modes in the fluctuation determinant around the instanton, and are

$$\beta_\omega \equiv \beta_\beta + 1 = \frac{1}{2}(D + 5 + N), \quad \beta_\eta = \frac{1}{2}(D + 1 + N), \quad \beta_{\bar\eta} = \frac{1}{2}(D + 3 + N). \tag{20.73}$$

The prefactors $\gamma_\beta, \gamma_\eta, \gamma_{\bar\eta}$ in (20.68)–(20.70) require the calculation of the full fluctuation determinants. This yields for γ_β the somewhat lengthy expression

$$\gamma_\beta \equiv \frac{(n+8)2^{(n+D-5)/2}3^{-3(D-2)/2}}{\pi^{3+D/2}\Gamma\left(2+\frac{1}{2}n\right)}\left(\frac{I_1^2}{I_4}\right)^2\left(\frac{I_6}{I_4}-1\right)^{D/2} D_L^{-1/2} D_T^{-(n-1)/2} e^{-1/a}. \tag{20.74}$$

The constants I_1, I_2, I_6 are generalizations of the above integral I_4:

$$I_p \equiv \int d^D x [\varphi_c(\mathbf{x})]^p, \tag{20.75}$$

and D_L and D_T are found from the longitudinal and transverse parts of the fluctuation determinants. Their numerical values are given in Table 20.3 . The constant γ_β is the prefactor of growth in the expansion coefficients of the β-function

$$f_k^\beta \approx \gamma_\beta (-\alpha)^k k! \Gamma(k + \beta_\beta + 1). \tag{20.76}$$

The prefactors in γ_ω, γ_η, and $\gamma_{\bar\eta}$ in (20.68)–(20.70) are related to γ_β by

$$\gamma_\omega = -\alpha\gamma_\beta, \qquad \gamma_\eta = \gamma_{\bar\eta} \frac{2H_3}{I_1 D(4-D)}, \qquad \gamma_{\bar\eta} = \gamma_\beta \frac{n+2}{n+8}(D-1)4\pi \frac{I_2}{I_1^2}, \tag{20.77}$$

where $I_2 = (1 - D/4)I_4$ and H_3 are listed in Table 20.3 . The numerical values of all growth

TABLE 20.4 Growth parameter of $D = 3$ perturbation expansions of $\beta(\bar g)$, $\eta(\bar g)$ and $\bar\eta = \eta + \nu^{-1} - 2$.

	$N=0$	$N=1$	$N=2$	$N=3$
a	0.1662460	0.14777422	0.1329968	0.12090618
β_ω	4	9/2	9	11/2
$\beta_{\bar\eta}$	3	7/2	4	9/2
β_η	2	5/2	3	7/2
$10^2 \times \gamma$	8.5489(16)	3.9962(6)	1.6302(3)	0.59609(10)
$10^3 \times \gamma_{\bar\eta}$	10.107	6.2991	3.0836	1.2813
$10^3 \times \gamma_\eta$	2.8836	1.7972	0.8798	0.3656

parameters are listed in Table 20.4 . In Fig. 20.22 we show a comparison between the exact coefficients and their asymptotic forms (20.70).

It is possible to use the information coming from the theoretical large-order behavior (20.68)–(20.70) to *predict* approximately the values of the expansion coefficients beyond the seven-loop order. For this we choose the coefficients $c^{(i)}$ in the asymptotic formulas (20.68)–(20.70) to fit exactly the six known expansion coefficients of $\omega(\bar g)$ and the seven of $\bar\eta(\bar g)$ and $\eta(\bar g)$. The coefficients are listed in Table 20.8 . The quality of the fits can be seen in Fig. 20.22.

Note that even and odd coefficients f_k^η lie on two smooth separate curves, so that we fit the two sets separately. These fits permit us now to extend the list of presently available coefficients as shown in Table 20.5 up to g^{20}. The errors in these predictions are expected to be smallest for f_k^ω, as illustrated in Fig. 20.23.

At this place we observe an interesting phenomenon. According to Table 20.5 , the expansion coefficients f_k^ω of $\omega(\bar g)$ have alternating signs and grow rapidly, reaching precociously their asymptotic form (20.68), as visible in Fig. 20.22. Now, from $\omega(\bar g)$ we can derive the so called β-function, $\beta(\bar g) \equiv \int d\bar g\, \omega(\bar g)$, and from this the expansion for the bare coupling constant $\bar g_B(\bar g) = -\int d\bar g/\beta(\bar g)$, with coefficients $f_k^{\bar g_0}$ listed in Table 20.6 . From the standard instanton analysis we know that the function $\bar g_0(\bar g)$ has the same left-hand cut in the complex $\bar g$-plane as the functions $\omega(\bar g), \bar\eta(\bar g), \eta(\bar g)$, with the same discontinuity proportional to $e^{-\text{const}/g}$ at the tip of the cut.

TABLE 20.5 Coefficients of extended perturbation expansions obtained from large-order expansions (20.68)–(20.70) for ω, $\bar{\eta} \equiv \nu^{-1} + \eta - 2$, η up to g^{12}.

	k	$N=0$	$N=1$	$N=2$	$N=3$
f_k^{ω}	0	-1	-1	-1	-1
	1	2	2	2	2
	2	-95/72	-308/243	-272/225	-1252/1089
	3	1.559690758	1.404278391	1.259667768	1.131786725
	4	-2.236580484	-1.882634142	-1.589642400	-1.351666500
	5	3.803133000	2.973285060	2.346615000	1.875335400
	6	-7.244496000	-5.247823000	-3.867143000	-2.904027000
	7	15.0706772	10.0938530	6.9384728	4.8954471
	8	-33.8354460	-20.9045761	-13.3833570	-8.8630280
	9	81.4263429	46.2983010	27.5543342	17.1018561
	10	-209.0371337	-109.1428445	-60.2679848	-34.9985085
	11	570.2558985	272.8574773	139.5403648	75.6925030
	12	−1647.63898	−721.159283	−340.986931	−172.506443
	13	5027.12671	2009.473994	877.142753	413.269514
	14	−16154.2792	−5888.53514	−2369.63316	−1038.433113
	15	54539.7867	18105.83253	6708.76515	2731.28823
	16	−193034.402	−58292.0930	−19865.5739	−7505.78230
	17	714771.195	196130.5369	61414.0151	21513.8526
	18	2.7637289×10^6	−688418.829	−197883.530	−64215.5872
	19	1.1139530×10^7	2.5166119×10^6	663509.086	199303.824
	20	-4.6728706×10^7	-9.5668866×10^6	-2.3117713×10^6	−642301.398
$f_k^{\bar{\eta}}$	1	-1/4	-1/3	-2/5	-5/11
	2	1/16	2/27	2/25	10/121
	3	-0.0357672729	-0.0443102531	-0.0495134446	-0.0525519564
	4	0.0343748465	0.0395195688	0.0407881055	0.0399640005
	5	-0.0408958349	-0.0444003474	-0.0437619509	-0.0413219917
	6	0.0597050472	0.0603634414	0.0555575703	0.0490929344
	7	-0.09928487	-0.09324948	-0.08041336	-0.06708630
	8	0.18143353	0.15857090	0.12955711	0.10413882
	9	-0.35946458	-0.29269274	-0.22839265	-0.17925852
	10	0.76759881	0.58218392	0.43525523	0.33488318
	11	-1.75999735	-1.24181846	-0.88911482	-0.66904757
	12	4.31887516	2.82935836	1.93487570	1.41644564
	13	−11.3068155	−6.86145603	−4.46485563	−3.15991301
	14	31.4831400	17.65348358	10.8846651	7.40110473
	15	−92.9568675	−48.04185493	−27.9476939	−18.1528875
	16	290.205144	137.9015950	75.3808299	46.5326521
	17	−955.369710	−416.4425396	−213.088140	−124.454143
	18	3308.08653	1319.8954890	630.008039	346.784997
	19	−12019.6749	−4380.9238169	−1944.51060	−1005.36571
	20	45726.095	15196.764595	6254.75115	3028.67211
f_k^{η}	1	0	0	0	0
	2	1/108	8/729	8/675	40/3267
	3	0.0007713749	0.0009142223	0.0009873600	0.0010200000
	4	0.0015898706	0.0017962229	0.0018368107	0.0017919257
	5	-0.0006606149	-0.0006536980	-0.0005863264	-0.0005040977
	6	0.0014103421	0.0013878101	0.0012513930	0.0010883237
	7	-0.001901867	-0.0016976941	-0.001395129	-0.001111499
	8	0.003178395	0.0026439888	0.002043629	0.001544149
	9	-0.006456700	-0.0049783320	-0.003585593	-0.002532983
	10	0.012015200	0.0084255120	0.005570210	0.003647578
	11	-0.029656348	-0.0194143738	-0.012066168	-0.007451622
	12	0.064239639	0.0378738590	0.021403479	0.012148673
	13	−0.180415293	−0.0992734993	−0.0527914785	−0.0282931664
	14	0.4519047994	0.22304200134	0.10748443321263	0.0528085190
	15	−1.4092869972	−0.6472476781	−0.2928360472879924	−0.135567321
	16	4.0214900375	1.65386975	0.677414388712502	0.287414739
	17	−13.7588144054	−5.24609037	−2.01071514	−0.801301742
	18	44.0902845294	15.0426293	5.21919799	1.907241838
	19	−164.205876	−51.7544723	−16.7458885	−5.728643910
	20	583.728411	164.571258	48.2146655	15.13540671

TABLE 20.6 Coefficients $f_k^{\bar{g}_B}$ of expansion $\bar{g}_B(\bar{g}) = \sum_{k=1}^{20} f_k^{\bar{g}_B} \bar{g}^k$, defining extended perturbation expansions deduced from large-order expansions (20.68)–(20.70) for $\omega(\bar{g})$.

k	$N=0$	$N=1$	$N=2$	$N=3$
1	1	1	1	1
2	+1	+1	+1	+1
3	+337/432	+575/729	+539/675	+2641/3267
4	+0.61685694588	+0.62411053351	+0.63484885720	+0.64721832545
5	+0.44266705709	+0.45557995443	+0.47149516705	+0.48876206059
6	+0.35597494073	+0.35927512536	+0.36876801981	+0.38195333853
7	+0.21840619207	+0.23668638696	+0.25507866294	+0.27372501773
8	+0.23516444398	+0.22010271935	+0.21833333377	+0.22423492600
9	+0.02522653990	+0.07797541233	+0.11146939079	+0.13619054953
10	+0.32466738893	+0.21722566733	+0.17071122132	+0.15281461436
11	−0.46084539160	−0.17781419227	−0.04796874299	+0.01851106465
12	+1.36111296151	+0.62177013621	+0.32371445346	+0.19688967179
13	−3.42004319798	−1.33935153089	−0.55625249070	−0.23297770291
14	+9.68597708110	+3.55457753745	+1.44715002648	+0.65263956302
15	−28.5286709455	−9.51594412468	−3.51833733708	−1.41477489238
16	+88.9376821020	+27.1477264424	+9.31404148366	+3.53850316476
17	−291.235785543	−81.0609653416	−25.6008150903	−9.00262320492
18	+1000.66241399	+253.799830529	+73.8458792207	+24.1544067361
19	−3599.15484483	−830.784519325	−222.359395181	−67.4743858406
20	+13526.5566605	+2838.71379781	+698.348588943	+196.518945901

TABLE 20.7 Coefficients $f_k^{\bar{g}}$ of expansion $\bar{g}(\bar{g}_B) = \sum_{k=1}^{20} f_k^{\bar{g}} \bar{g}_B^k$, obtained by inverting the extended series in Table 20.6 .

k	$N=0$	$N=1$	$N=2$	$N=3$
1	1	1	1	1
2	−1	−1	−1	−1
3	+527/432	+883/729	+811/675	+3893/3267
4	−1.7163939829	−1.680351960126292	−1.642256264617284	−1.60528382897736
5	+2.7021635328	+2.591685040643859	+2.481604560563785	+2.378891143794822
6	−4.6723281932	−4.363908063002809	−4.073635397816119	−3.813515390028028
7	+8.7648283753	+7.926093595753771	+7.180326093595318	+6.539645290718699
8	−17.684135663	−15.39841276963578	−13.47981441366666	−11.90293506879397
9	+38.129348202	+31.80063328573243	+26.79259688548747	+22.86325133485651
10	−87.419391225	−69.48420478282783	−56.1279351033013	−46.14596304145893
11	+212.28789113	+160.0400066477353	+123.4985362910675	+97.5437851896555
12	−544.33806227	−387.4479410496121	−284.6297746951519	−215.3826650602743
13	+1470.2445538	+983.719405302971	+685.668309006505	+495.7770927688912
14	−4175.1804881	−2614.933427024693	−1723.672999416843	−1187.794187410145
15	+12447.739474	+7268.064649337187	+4516.120357408118	+2958.336103932099
16	−38915.141370	−21101.49568383381	−12320.85534817637	−7652.516371929849
17	+127440.33105	+63943.24392789235	+34975.98186824855	+20545.02631707489
18	−436738.21140	−202094.1329180427	−103252.1798678474	−57215.98372843337
19	+1564637.2472	+665710.523944826	+316810.7604431689	+165210.8008728902
20	−5853354.4104	−2283830.09806744	−1009811.938755735	−494409.476944406

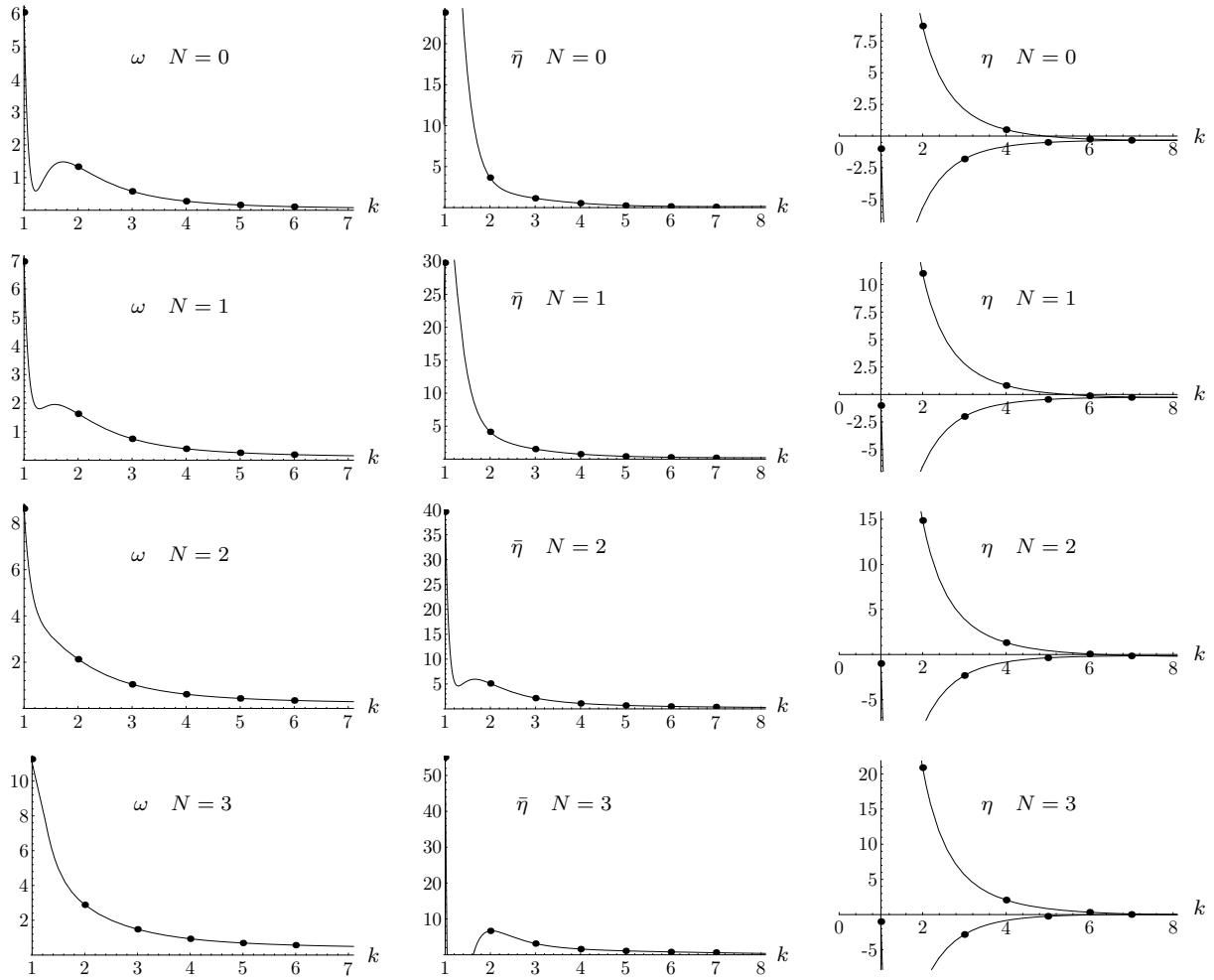

FIGURE 20.22 Early onset (precocity) of large-order behavior of coefficients of the expansions of the critical exponents ω, η, and $\bar{\eta} \equiv \nu^{-1} + \eta - 2$ in powers of the renormalized coupling constant. The dots show the relative deviations (exact value)/(asymptotic value) – 1. The curves are plots of the asymptotic expressions in Eqs. (20.68)–(20.70) listed in Table 20.8 . The curve for ω is the smoothest, promising the best extrapolation to the next orders, with consequences to be discussed in Section 20.6.

Hence the coefficients $f_k^{\bar{g}_0}$ must have asymptotically similar alternating signs and a factorial growth. Surprisingly, this expectation is not borne out by the explicit seven-loop coefficients $\bar{g}_0^{(k)}$ following from (20.68) in Table 20.6 . However, if we look at the higher-order coefficients derived from the extrapolated f_k^{ω} sequence which are also listed in that table, we see that sign change and factorial growth do eventually set in at the rather high order 11. Before this order, the coefficients $f_k^{\bar{g}_0}$ look like those of a convergent series. If we were to make a plot analogous to those in Fig. 20.22 for $f_k^{\bar{g}_0}$, we would observe huge deviations from the asymptotic form up to an order much larger than 10. In contrast, the inverse series $\bar{g}(\bar{g}_0)$ has expansion coefficients $f_k^{\bar{g}}$ which do approach rapidly their asymptotic form, as seen in Table 20.7 . This is the reason why our resummation of the critical exponents $\omega, \bar{\eta}, \eta$ as power series in $\bar{g}_B$ already yields good results at the available low order seven.

TABLE 20.8 Coefficients of the large-order expansions (20.68)–(20.70) fitting known expansion coefficients of ω, η, $\bar{\eta}$. The coefficients f_k^η possess two separate expansions for even and odd k.

	N	$c^{(1)}$	$c^{(2)}$	$c^{(3)}$	$c^{(4)}$	$c^{(5)}$	$c^{(6)}$
ω	0	0.26301475112	3.4408182822	-31.76733359043	209.94304685908	-387.9820769504	212.1565739538
	1	1.63535099051	-8.7629408561	32.52987246310	49.56939798556	-198.5501186375	130.5393597659
	2	4.19032409932	-32.5218822010	159.23160834532	-271.56782378290	185.5214629862	-36.2203620935
	3	8.06590542355	-69.1380037623	356.19870179271	-773.40843073419	787.4105682986	-297.8631178069
$\bar{\eta}$	0	15.47452873233	-263.105249597	1695.8521799417	-4797.254788814	6198.211268910	-2825.378774427
	1	10.94704206385	-169.697930580	1074.8269224230	-2886.578089415	3577.486553055	-1577.198376659
	2	1.24814548715	60.9324565140	-409.5953535647	1526.620407734	-2300.494640749	1163.425537324
	3	-25.80328671245	508.523659337	-3253.9391201198	9876.171576908	-13307.48621904	6257.590654494
$\eta_{\rm o}$	0	-6.363429671227	54.7969857339	-209.2126943952	159.77913833249		
	1	-5.860815634115	58.1732922278	-237.1581744239	183.84569783020		
	2	-5.108698105700	64.4651051506	-285.1161542307	224.75974718583		
	3	-4.203986342723	76.2691471289	-364.4529959457	291.38783515954		
$\eta_{\rm e}$	0	-5.6929922203758	15.551243915764	61.12469347544379			
	1	-5.3245881267711	14.110708087849	81.2312043328075			
	2	-4.5203425601138	9.799960635959	117.4131477198922			
	3	-3.1970976073075	1.705210978430	176.4615812743069			

20.6 Influence of Large-Order Information

The critical exponents obtained so far have quite a high accuracy. The question arises whether this can be increased further by making use of the extended set of expansion coefficients in Table 20.5 derived from the theoretically known large-order behavior (20.68)–(20.70). We shall now demonstrate that the gain of accuracy is very modest. Within strong-coupling theory, the knowledge of the large-order behavior has little influence on the results except for ω whose values are slightly lowered (by less than $\sim 0.2\%$). The reason for this seems to be that in the present approach the critical exponents are obtained from evaluations of expansions at infinite bare couplings. The information on the large-order behavior, on the other hand, specifies the discontinuity at the tip of the left-hand cut at the origin of the complex-coupling constant plane, which is too far from the infinite-coupling limit to be of relevance. The use of ω-information in our extrapolation is crucial to obtaining high accuracy when resumming the series in the bare coupling constant. This information is more useful than the large-order information in previous resummation schemes in which the critical exponents are determined at a finite renormalized coupling constant g^* of order unity, which lies at a finite distance from the left-hand cut in the complex g-plane. Although this determination is sensitive to the discontinuity at the tip of the cut, it must be realized that the influence of the cut is very small due to the smallness of the *fugacity* of the leading instanton, which is equal to a Boltzmann factor $e^{-\text{const}/g}$.

Let us see the results obtained by using the extended list of expansion coefficients in Table 20.5 . The extrapolations are shown in Fig. 20.24, for an extension of the known six-loops coefficients of $\omega(\bar{g}_B)$ and $\eta(\bar{g}_B)$ by one extrapolated coefficient. This produces an even number of approximants which can be most easily extrapolated to infinite order. For $\bar{\eta}(\bar{g}_B)$ we use two more coefficients for the same reason. The resulting ω_8-values are lowered somewhat with respect to ω_6 from (20.61) to

$$\omega_8 = \left\{ \begin{array}{l} 0.7935 \\ 0.7916 \\ 0.7900 \\ 0.7880 \end{array} \right\} \quad \text{for} \quad \left\{ \begin{array}{l} N=0 \\ N=1 \\ N=2 \\ N=3 \end{array} \right\}. \tag{20.78}$$

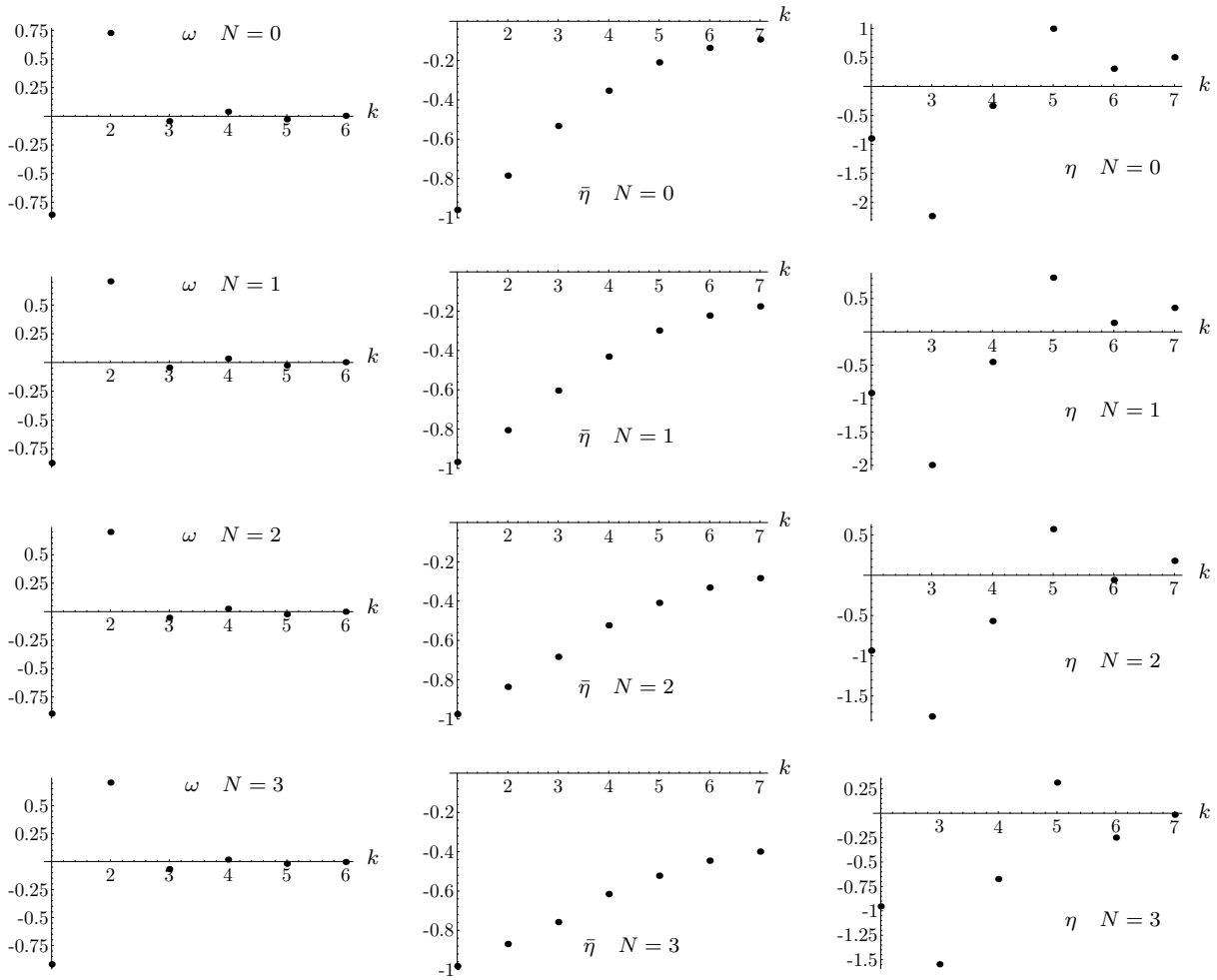

FIGURE 20.23 Relative errors $f_k/f_k^{\text{large order}} - 1$ in predicting the kth expansion coefficient by fitting the large-order expressions (20.68)–(20.70) for ω, , η, and $\bar{\eta} \equiv \nu^{-1} + \eta - 2$ to the first $k-1$ expansion coefficients.

The new η values are

$$\eta_8 = \left\{ \begin{array}{l} 0.02829 - 0.01675 \times (\omega - 0.7935) \\ 0.03319 - 0.01523 \times (\omega - 0.7916) \\ 0.03503 - 0.02428 \times (\omega - 0.7900) \\ 0.03537 - 0.01490 \times (\omega - 0.7880) \end{array} \right\} \quad \text{for} \quad \left\{ \begin{array}{l} N = 0 \\ N = 1 \\ N = 2 \\ N = 3 \end{array} \right\}, \tag{20.79}$$

lying reasonably close to the previous seven-loop results (20.63), (20.64) for the smaller ω-values (20.78). The first set yields $\eta_8 = \{0.0300, 0.0356, 0.0360, 0.0354\}$; the second $\eta_8 = \{0.0315, 0.0342, 0.0349, 0.0345\}$.

For $\bar{\eta}$ we find the results

$$\bar{\eta}_9 = \left\{ \begin{array}{l} -0.2711 + 0.0400 \times (\omega - 0.810) \\ -0.3803 + 0.0974 \times (\omega - 0.805) \\ -0.4735 + 0.1240 \times (\omega - 0.800) \\ -0.5506 + 0.4761 \times (\omega - 0.797) \end{array} \right\} \quad \text{for} \quad \left\{ \begin{array}{l} N = 0 \\ N = 1 \\ N = 2 \\ N = 3 \end{array} \right\}. \tag{20.80}$$

It is interesting to observe how the resummed values $\omega_L, \bar{\eta}_L, \eta_L$ obtained from the extrapolated expansion coefficients in Table 20.5 continue to higher orders in N. This is shown in

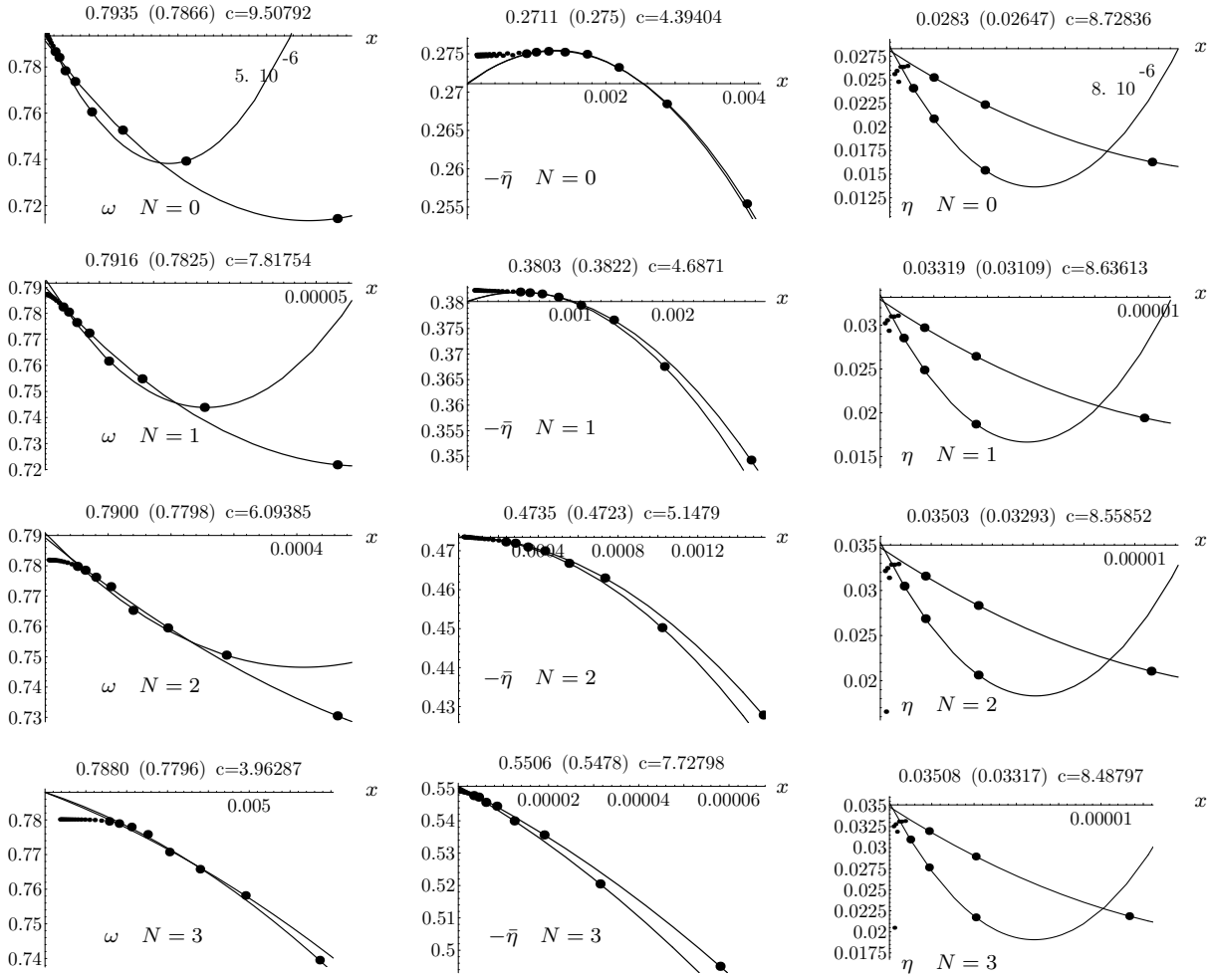

FIGURE 20.24 Extrapolation of resummed $\omega, \bar{\eta}, \eta$-values if one (ω, η) or two $(\bar{\eta})$ more expansion coefficients of Table 20.5 are taken into account. The fat dots show the resummed values used for extrapolation, the small dots higher resummed values not used for the extrapolation. The numbers on top specify the extrapolated values and the values of the last approximation, corresponding to the leftmost fat dot.

Fig. 20.25. The dots converge to some specific values which, however, are different from the extrapolation results in Fig. 20.24 based on the theoretical convergence behavior error $\approx e^{-cN^{1-\omega}}$. We shall argue below that these results are worse than the properly extrapolated values.

All the above numbers agree reasonably well with each other and with other estimates in the literature listed in Table 20.1 on page 375. The only comparison with experiment which is sensitive enough to judge the accuracy of the results and the reliability of the resummation procedure is provided by the measurement of the critical exponent $\alpha = 2 - 3\nu$ in the space shuttle experiment of Lipa et al. [16] whose data were plotted in Fig. 1.2. By going into a vicinity of the critical temperature with $\Delta T \approx 10^{-8}$ K, their fit to the experimental singularity $C \propto |1 - T/T_c|^{-\alpha}$ in the specific heat at the λ-point of superfluid helium, yields the highly accurate value [recall Eq. (1.23)]

$$\alpha = -0.01056 \pm 0.00038. \tag{20.81}$$

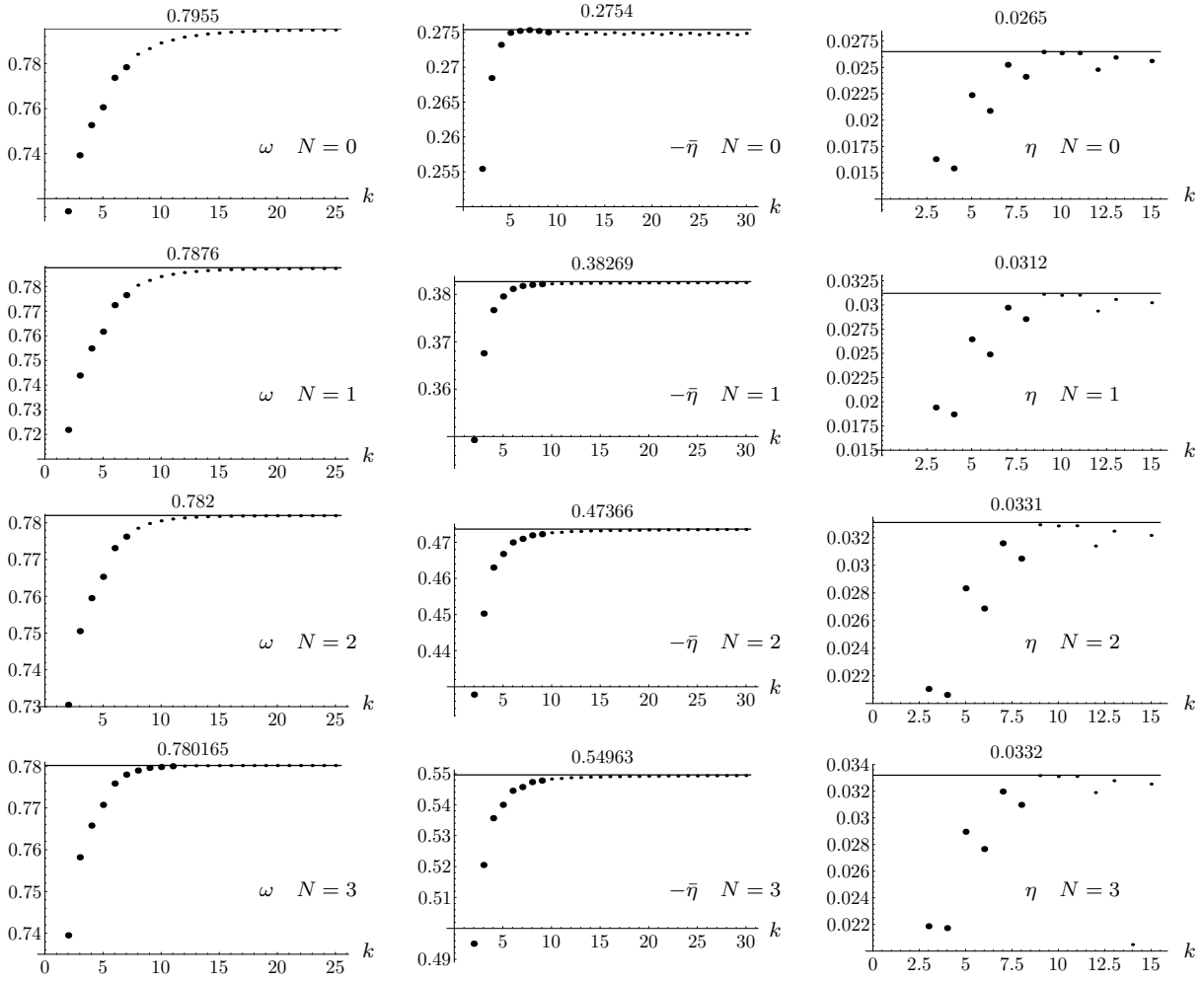

FIGURE 20.25 Direct plots of the resummed $\omega, \bar{\eta}, \eta$-values for all resummed values from all extrapolated expansion coefficients of Table 20.5 . The line is fitted to the maximum of all dots at the place specified by the number on top. Fat and small dots distinguish the resummed exponents used in the previous extrapolations from the unused ones.

Since ν is of the order 2/3, this measurement is extremely sensitive to ν, which is

$$\nu = 0.6702 \pm 0.0001. \tag{20.82}$$

It is therefore useful to perform resummation and extrapolation at $N = 2$ directly for the approximate α-values $\alpha_L = 2 - 3\nu_L$, once for the six-loop ω-value $\omega = 0.8$, and once for a neighboring value $\omega = 0.790$, to see the ω-dependence. The results are shown in Fig. 20.26. The extrapolated values for our $\omega = 0.8$ in Table 20.1 on page 375 yield

$$\alpha = -0.01294 \pm 0.00060, \tag{20.83}$$

in very good agreement with experiment.

Note that the results get worse if we use more than eleven orders of the extended series. This shows that the higher extrapolated expansion coefficients in Table 20.5 do not really carry more information on the critical exponent ν. Although these coefficients lie closer and closer to the true ones as expected from the decreasing errors in the plots in Fig. 20.23, this does not

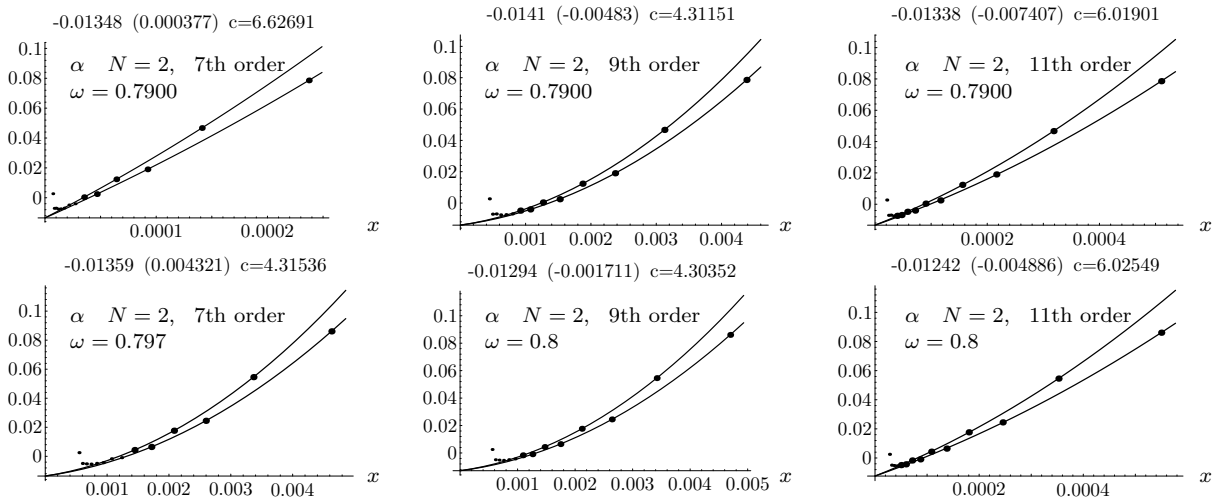

FIGURE 20.26 Extrapolation of resummed α-values if two more expansion coefficients are used from Table 20.5. The small dots near the origins show how the resummed results start deviating from the smooth exptrapolation curve if more than two coefficients are taken into account.

increase their usefulness. The errors are samll only in relation to the huge factorially growing expansion coefficients. The resummation procedure removes the factorial growth and becomes extremely sensitive to very small deviations from these huge coefficients. This is the numerical consequence of the fact discussed earlier that the information residing in the exponentially small imaginary part of all critical exponents near the tip of the left-hand cut in the complex $\bar{g}_B$-plane has practically no effect upon the strong-coupling results at infinite $\bar{g}_B$.

Therefore, the knowledge of the large-order behavior is only of limited help in improving the accuracy of the approximation. In our theory, an additional important information is contained in the theoretically known exponential convergence behavior which predicts a linear behavior of the approximations when plotted against $x(L) = e^{-cL^{1-\omega}}$. This knowledge, which allows us to extrapolate our approximations for $L = 2, 3, 4, 5, 6, 7$ well to infinite order L, seems to be more powerful than that of the large-order behavior.

The complete updated list of exponents is shown in Table 20.2 , which also contains values for the other critical exponents $\alpha = 2 - D\nu$ and $\beta = \nu(D - 2 + \eta)/2$.

A further improvement of the above results should be possible by taking into account the existence of further terms $1/g_B^{\omega'}$, $(1/g_B^{2\omega'}), \ldots$ in the strong-coupling expansion (19.52), corresponding to *confluent singularities* [17] in the renormalized coupling constant $\bar{g}$. This can be done following the strategy developed for simple quantum-mechanical systems [18].

20.7 Another Variational Resummation Method

With the experimental value of α offering a sensitive method for the quality of various resummation schemes, let us also try another such scheme based on variational perturbation theory [19]. Consider the seven-loop power series expansion for $\nu^{-1}(\bar{g}_B) = 2 - \eta_m(\bar{g}_B)$ in powers of the unrenormalized coupling constant of O(2)-invariant ϕ^4-theory [recall Eqs. (20.18) and (20.60)]:

$$\begin{aligned} \nu^{-1} &= 2 - 0.4\,\bar{g}_B + 0.4681481481482289\,\bar{g}_B^2 - 0.66739\,\bar{g}_B^3 + 1.079261838589703\,\bar{g}_B^4 \\ &- 1.91274\,\bar{g}_B^5 + 3.644347291527398\,\bar{g}_B^6 - 7.37808\,\bar{g}_B^7 + \ldots\ . \end{aligned} \tag{20.84}$$

Using the fits in Tables 20.8 to the theoretical large-order behavior we extend this series to higher orders as follows (see Table 20.5) [20]:

$$\begin{aligned}\Delta\nu^{-1} &= 15.75313406543747\,\bar{g}_B^8 - 35.2944\,\bar{g}_B^9 + 82.6900901520064\,\bar{g}_B^{10} \\ &- 202.094\,\bar{g}_B^{11} + 514.3394395526179\,\bar{g}_B^{12} - 1361.42\,\bar{g}_B^{13} \\ &+ 3744.242656157152\,\bar{g}_B^{14} - 10691.7\,\bar{g}_B^{15} + \dots\ . \end{aligned} \tag{20.85}$$

We now calculate the expansion for the logarithmic derivative $s = \bar{g}_B\bar{g}'(\bar{g}_B)/\bar{g}(\bar{g}_B)$ [recall (19.61)] of the renormalized coupling constant in powers of $\bar{g}_B$ from (20.15):

$$\begin{aligned}s &= 1 - \bar{g}_B + \frac{947\,\bar{g}_B^2}{675} - 2.322324349407407\,\bar{g}_B^3 + 4.276203609026057\,\bar{g}_B^4 \\ &- 8.51611440473227\,\bar{g}_B^5 + 18.05897631325589\,\bar{g}_B^6 + \dots\ . \end{aligned} \tag{20.86}$$

A fit with the theoretical large-order behavior extends this series by [see Table (20.7)]

$$\begin{aligned}\Delta s &= 40.386572287301\,\bar{g}_B^7 + 94.645339912347\,\bar{g}_B^8 - 231.39224421625\,\bar{g}_B^9 \\ &+ 588.32061725791\,\bar{g}_B^{10} - 1552.1163584042\,\bar{g}_B^{11} + 4242.3726850801\,\bar{g}_B^{12} \\ &- 12001.188664918\,\bar{g}_B^{13} + 35115.230066461\,\bar{g}_B^{14} - 106234.46430864\,\bar{g}_B^{15} + \dots\ . \end{aligned} \tag{20.87}$$

The scaling properties of the theory near T_c imply that $g(\bar{g}_B)$ becomes a constant for $\bar{g}_B \to \infty$, so that $s(\bar{g}_B)$ goes to zero in this limit. By inverting the expansion for $s(\bar{g}_B) + \Delta s(\bar{g}_B)$, we obtain an expansion for $\bar{g}_B$ in powers of $h \equiv 1 - s$, and subsequently from (20.84), (20.85) an expansion for ν^{-1} in powers of $h \equiv 1 - s$ as follows:

$$\begin{aligned}\nu^{-1}(h) &= 2 - 0.4\,h - 0.093037\,h^2 + 0.000485012\,h^3 - 0.0139286\,h^4 + 0.007349\,h^5 - 0.0140478\,h^6 \\ &+ 0.0159545\,h^7 - 0.029175\,h^8 + 0.0521537\,h^9 - 0.102226\,h^{10} + 0.224026\,h^{11} - 0.491045\,h^{12} \\ &+ 1.22506\,h^{13} - 3.00608\,h^{14} + 8.29528\,h^{15} + \dots\ . \end{aligned} \tag{20.88}$$

The critical exponent ν^{-1} is obtained by evaluating this series at $h = 1$ via variational perturbation theory. From the result we obtain the critical exponent $\alpha = 2 - 3\nu$.

For estimating the systematic errors of our resummation, we also re-expand (20.88) to find the corresponding power series for $\alpha = 2 - 3\nu$:

$$\begin{aligned}\alpha(h) &= 0.5 - 0.3\,h - 0.129778\,h^2 - 0.0395474\,h^3 - 0.0243203\,h^4 - 0.0032498\,h^5 - 0.0121091\,h^6 \\ &+ 0.00749308\,h^7 - 0.0194876\,h^8 + 0.0320172\,h^9 - 0.0651726\,h^{10} + 0.14422\,h^{11} - 0.315055\,h^{12} \\ &+ 0.802395\,h^{13} - 1.95455\,h^{14} + 5.49143\,h^{15} + \dots\ , \end{aligned} \tag{20.89}$$

whose value at $h = 1$ gives directly the critical exponent α, from which we obtain another approximation for $\nu = (2 - \alpha)/3$.

In order to obtain a first idea of the behavior of the expansions (20.88) and (20.89), we plot their partial sums at $h = 1$ in the upper row of Fig. 20.27. After an initial apparent convergence, the partial sums show the typical divergence of asymptotic series which call for a resummation. A rough resummation is possible using Padé approximants. The results are shown in Table 20.9 . The highest Padé approximants yield

$$\alpha^{\mathrm{P}} = -0.0123 \pm 0.0050. \tag{20.90}$$

The error is estimated by the distance from the next lower approximation.

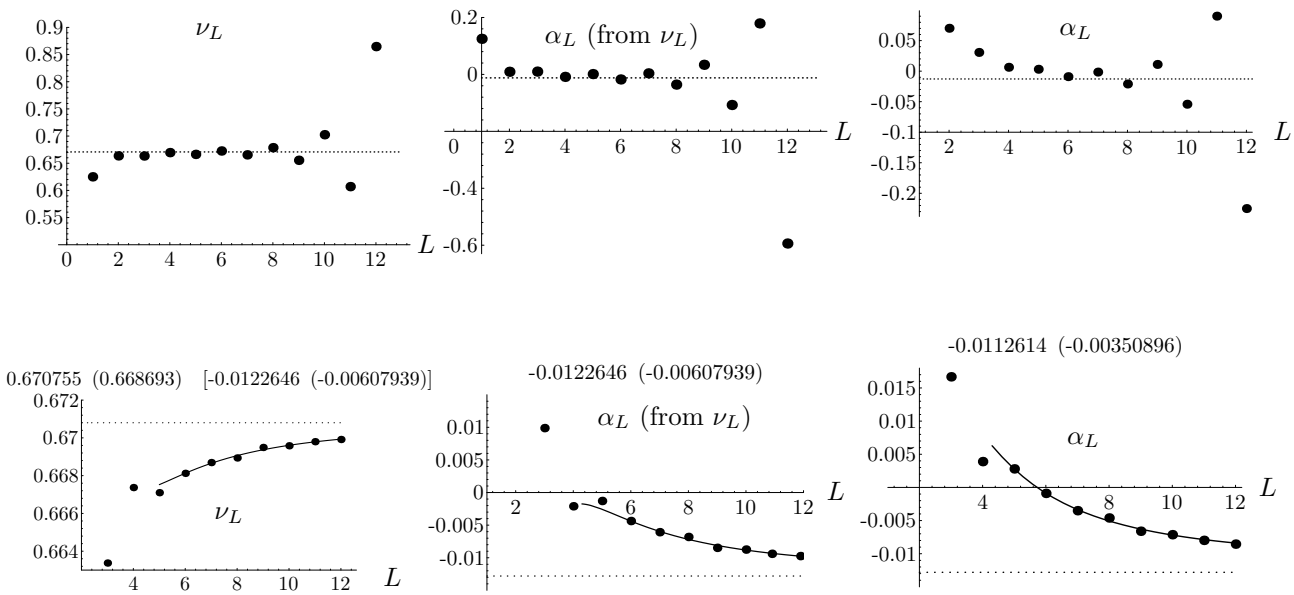

FIGURE 20.27 Upper plots: Results of partial sums of series (20.88) for $\nu^{-1}(h=1)$ up to order L, once plotted as $\nu_L = 1/\nu_L^{-1}$, and once as $\alpha_L = 2 - 3\nu_L$. The right-hand plot shows the corresponding partial sums of the series (20.89) for $\alpha(h=1)$. The dotted lines indicate the experimental value $\alpha^{\rm ss} = -0.01285 \pm 0.00038$ of the space shuttle data in Fig. 1.2. Lower plots: The corresponding resummed values and a fit of them by $c_0 + c_1/L^2 + c_2/L^4$. The constant c_0 is written on top, together with the seventh-order approximation (in parentheses). The square brackets on top of the left-hand plot for ν shows the corresponding α-values.

We now resum the expansions (20.88) and (20.89) by variational perturbation theory. Since we now want to know the functions at a finite argument h, we cannot use (19.16) but must first adapt our function to the general form to which we can apply our resummation procedure. Plotting the successive truncated power series for $\nu^{-1}(h)$ against h in Fig. 20.28, we see that this function curve seems to have a zero somewhere above $h = h_0 = 3$. We therefore go over to the variable x defined by $h = h(x) \equiv h_0 x/(h_0 - 1 + x)$, in terms of which $f(x) = \nu^{-1}(h(x))$. It has a power series expansion

$$f(x) = \sum_{n=0}^{\infty} f_n x^n, \tag{20.91}$$

TABLE 20.9 Results of Padé approximations $P_{MN}(h)$ at $h = 1$ to power series $\nu^{-1}(h)$ and $\alpha(h)$ in Eq. (20.88) and Eq. (20.89), respectively. The parentheses show the associated values of α and ν.

MN	ν (α)	(ν) α
4 4	0.678793 (-0.0363802)	(0.678793) -0.0363802
5 4	0.671104 (-0.0133107)	(0.670965) -0.0128940
4 5	0.670965 (-0.0128940)	(0.670901) -0.0127031
5 5	0.670756 (-0.0122678)	(0.670756) -0.0122678

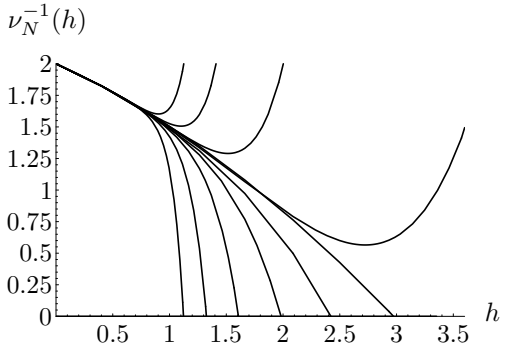

FIGURE 20.28 Successive truncated expansions of $\nu^{-1}(h)$ of orders $N = 2, \ldots, 12$.

which behaves like (20.9) with $p = 0$ and $q = 2$, and has to be evaluated at $x = 1$ corresponding to $\bar{g}_B = 0$. This large-x behavior is obtained in the resummation of (20.91) by introducing an auxiliary scale parameter κ and forming the truncated functions

$$f_L(x) \equiv \kappa^p \sum_{n=0}^{L} f_n \left(\frac{x}{\kappa^q}\right)^n . \tag{20.92}$$

The parameter κ will be set equal to 1 at the end. Then we introduce a variational parameter K by the replacement

$$\kappa \to \sqrt{K^2 + \kappa^2 - K^2}. \tag{20.93}$$

The functions $f_L(x)$ are so far independent of K. This is changed by expanding the square root in (20.93) in powers of $\kappa^2 - K^2$, thereby treating this quantity as being of order h. The terms $\kappa^p x^n/\kappa^{qn}$ in (20.92) are then expanded as

$$\kappa^p \frac{x^n}{\kappa^{qn}} \to K^p \frac{x^n}{K^{qn}} \left[1 + \binom{(p-qn)/2}{1} r + \binom{(p-qn)/2}{2} r^2 + \ldots + \binom{(p-qn)/2}{N-n} r^{N-n}\right], \tag{20.94}$$

where $r = (\kappa^2 - K^2)/K^2$. Setting $\kappa = 1$ and replacing the variational parameter K by v defined by $K^2 \equiv v^{-1}x$, we obtain from (20.92) at $x = 1$ the variational expansions

$$W_L(1, K) = \sum_{n=0}^{L} f_n \, v^{qn-p/2} \, [1 - (1 - v)]_{L-n}^{(p-qn)/2} , \tag{20.95}$$

where the symbol $[1 - A]_{N-n}^{(p-qn)/2}$ was defined in Eq. (19.17) by the binomial expansion of $(1 - A)^{(p-qn)/2}$ in powers of A up to the order A^{N-n}. This is of course the expansion (19.6) in which the role of g_B is played by x. At $g_B \equiv x = 1$, the paramter $\sigma(K)$ in Eq. (19.5) is equal to $\sigma = (1 - 1/K^2)K^q$ at $\kappa = 1$, and $K^2 = v^{-1}$.

The appropriate modification of formula (19.16) for the evaluation at unit argument rather than the strong-coupling limit is

$$f_L^*(1) = \operatorname*{opt}_v \left[\sum_{l=0}^{L} f_l v^{l-p/2} \, [1 - (1 - v)]_{L-l}^{(p-ql)/2}\right]. \tag{20.96}$$

The variational expansions are listed in Table 20.10 . They are optimized in v by minima for odd and by turning points for even L, as shown in Fig. 20.29. The extrema are plotted as

TABLE 20.10 Variational expansions $\nu_L^{-1}(x)$ and $\alpha_L(x)$ for $L = 2, \ldots, 9$. They depend on the variational parameter K via $v = x/K^2$, and are plotted for $x = 1$ in Fig. 20.29. Their minima or turning points are extrapolated to $L = \infty$ in the lower plots of Fig. 20.27. The table goes only up to $L = 9$, to save space, the plots go to $L = 12$.

$$\nu_2^{-1} = 2 - 1.2v + 0.69067v^2$$
$$\nu_3^{-1} = 2 - 1.8v + 2.07200v^2 - 0.72036v^3$$
$$\nu_4^{-1} = 2 - 2.4v + 4.14400v^2 - 2.88145v^3 + 0.53412v^4$$
$$\nu_5^{-1} = 2 - 3.0v + 6.90667v^2 - 7.20363v^3 + 2.67060v^4 + 0.28949v^5$$
$$\nu_6^{-1} = 2 - 3.6v + 10.3600v^2 - 14.4073v^3 + 8.01180v^4 + 1.73692v^5 - 2.96286v^6$$
$$\nu_7^{-1} = 2 - 4.2v + 14.5040v^2 - 25.2127v^3 + 18.6942v^4 + 6.07922v^5 - 20.7401v^6 + 11.1835v^7$$
$$\nu_8^{-1} = 2 - 4.8v + 19.3387v^2 - 40.3403v^3 + 37.3884v^4 + 16.2113v^5 - 82.9602v^6 + 89.4683v^7 - 36.9575v^8$$
$$\nu_9^{-1} = 2 - 5.4v + 24.8640v^2 - 60.5105v^3 + 67.2992v^4 + 36.4753v^5 - 248.881v^6 + 402.607v^7 - 332.617v^8 + 121.914v^9$$

$$\alpha_2 = 0.5 - 0.90v + 0.3830v^2$$
$$\alpha_3 = 0.5 - 1.35v + 1.1490v^2 - 0.26997v^3$$
$$\alpha_4 = 0.5 - 1.80v + 2.2980v^2 - 1.07989v^3 + 0.025254v^4$$
$$\alpha_5 = 0.5 - 2.25v + 3.8300v^2 - 2.69972v^3 + 0.126271v^4 + 0.57604v^5$$
$$\alpha_6 = 0.5 - 2.70v + 5.7450v^2 - 5.39945v^3 + 0.378812v^4 + 3.45629v^5 - 2.19244v^6$$
$$\alpha_7 = 0.5 - 3.15v + 8.0430v^2 - 9.44903v^3 + 0.883895v^4 + 12.0970v^5 - 15.3471v^6 + 6.89011v^7$$
$$\alpha_8 = 0.5 - 3.60v + 10.724v^2 - 15.1184v^3 + 1.767790v^4 + 32.2587v^5 - 61.3884v^6 + 55.1208v^7 - 21.5704v^8$$
$$\alpha_9 = 0.5 - 4.05v + 13.788v^2 - 22.6777v^3 + 3.182020v^4 + 72.5821v^5 - 184.165v^6 + 248.044v^7 - 194.134v^8 + 70.781v^9$$

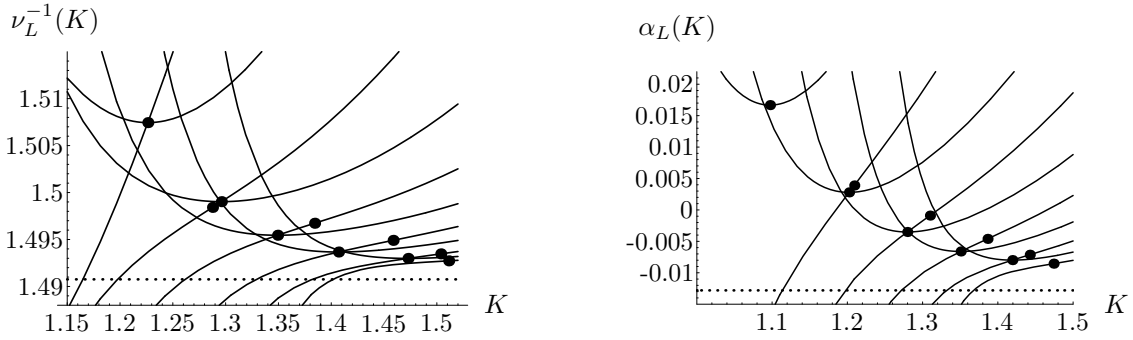

FIGURE 20.29 Successive variational functions $\nu_L^{-1}(h)$ and $\alpha_L(h)$ of Table 20.10 plotted for $h = x = 1$ against the variational parameter $K = \sqrt{x/v}$, together with their minima for odd L, or turning points for even L. These points are plotted against L in the lower row of Fig. 20.27, where they are extrapolated to $L \to \infty$, yielding the critical exponents.

a function of the order L in the lower row of Fig. 20.27. The left-hand plot shows directly the extremal values of $\nu_L^{-1}(v)$, the middle plot shows the α-values $\alpha_L = 2 - 3\nu_L$ corresponding to these. The right-hand plot, finally, shows the extremal values of $\alpha_L(v)$. All three sequences of approximations are fitted very well by a large L expansion $c_0 + c_1/L^2 + c_2/L^4$, if we omit the lowest five data points which are not yet very regular. The inverse powers of L were determined by making a general ansatz $c_0 + c_1/L^{p_1} + c_2/L^{p_2}$ and varying p_1, p_2 until the sum of the square deviations of the fit from the points is minimal. The highest data point is chosen to be the one with $L = 12$ since, up to this order, the successive asymptotic values c_0 change monotonously by decreasing amounts. Starting with $L = 13$, the changes increase and reverse direction. In addition, the mean square deviations of the fits increase drastically, indicating a decreasing usefulness of the extrapolated expansion coefficients in (20.85) and (20.87) for the extrapolation $N \to \infty$. From the parameter c_0 of the best fit for α which is indicated on top of the lower right-hand plot in Fig. 20.27, we find the critical exponent

$$\alpha = -0.01126 \pm 0.0010, \tag{20.97}$$

where the error estimate takes into account the basic systematic errors indicated by the difference between the resummation of $\alpha = 2 - 3\nu$, and of ν^{-1}, which by the lower middle plot in Fig. 20.27 yields $\alpha = -0.01226$. It also accommodates our earlier results from the previous seven-loop resummation in Ref. [20] for α in Eq. (20.83).

The dependence on the choice of h_0 is negligible as long as the resummed series $\nu^{-1}(x)$ and $\alpha(x)$ do not change their Borel character. Thus $h_0 = 2.2$ leads to results well within the error limits in (20.97). The critical exponent (20.97) is in excellent agreement with the experimental space shuttle value (20.81). A graphical comparison of our result with experiment and the results of numerous other authors will be given in the next chapter, in Fig. **??**.

As before, a further improvement of all resummation results should be possible by taking into account the existence of further terms $1/g_B^{\omega'}$, $(1/g_B^{\omega'})^2, \ldots$ in the strong-coupling expansion corresponding to confluent singularities [recall the remarks in Section 19.4] [17] in the renormalized coupling constant $\bar{g}$.

20.8 High-Temperature Expansions of Lattice Models

It is also possible to extract the critical value β_c directly from the following combination of ratios:

$$\beta_n = \left[nR_n - (n-1)R_{n-1}\right]^{-1}. \tag{20.98}$$

Since this combination contains no corrections of order $1/n$, we plot the sequence against $1/n^2$, with the results shown in Fig. 20.30. The critical exponent γ can be obtained most directly from the $n \to \infty$ -limit of the sequence

$$\gamma_n = 1 - n(n-1)\frac{R_n - R_{n-1}}{nR_n - (n-1)R_{n-1}}. \tag{20.99}$$

An alternative and more ancient access to critical exponents of the O(N) universality classes is possible via the classical Heisenberg model, whose energy has been given in Eq. (1.52). For this model, the literature has by now offered extensive high-temperature expansions. The basics of such models are explained in many textbooks [21]. The classical Heisenberg model has the partition function

$$Z(\beta) = \prod_i \int d\mathbf{S}(\mathbf{x}_i) \exp\left[\frac{\beta}{2}\sum_{\{i,j\}} \mathbf{S}(\mathbf{x}_i)\mathbf{S}(\mathbf{x}_j)\right], \tag{20.100}$$

where $\beta \equiv J/k_B T$ is the inverse temperature in natural units, $\mathbf{S}_i$ are unit vectors on the lattice sites $\mathbf{x}_i$ covered by the sum over i. For each i, the sum over j runs over all nearest neighbors of the site $\mathbf{x}_i$. The integrals $d\mathbf{S}(\mathbf{x}_i)$ cover the surface of an N-dimensional sphere.

For this model, several quantities have been calculated [23] on square, simple-cubic (sc), and body-centered cubic (bcc) lattices as a power series in β up to the order β^{22}. In particular, we know the susceptibility

$$\chi(\beta) = \sum_i \langle \mathbf{S}(\mathbf{x}_i)\mathbf{S}(\mathbf{x}_j)\rangle = 1 + \sum_{k=1}^{L} a_k \beta^k \tag{20.101}$$

up to order β^{22}. For $N = 2$ on a bcc lattice, $\chi(\beta)$ starts out like

$$\chi(\beta) = 1 + 8\,\frac{\beta}{2} + 56\left(\frac{\beta}{2}\right)^2 + 388\left(\frac{\beta}{2}\right)^3 + \dots\ . \tag{20.102}$$

Note that since the susceptibility diverges near β_c like $(\beta_c - \beta)^{-\gamma}$, and since the correlation function $\langle \mathbf{S}(\mathbf{x}_i)\mathbf{S}(\mathbf{x}_j)\rangle$ falls off exponentially with the correlation length like

$$\langle \mathbf{S}(\mathbf{x}_i)\mathbf{S}(\mathbf{x}_j)\rangle \approx g(\beta)\, e^{-|\mathbf{x}_i - \mathbf{x}_j|/\xi(\beta)}, \tag{20.103}$$

the prefactor diverges like

$$g(\beta) \approx (\beta_c - \beta)^{-\gamma+3\nu}. \tag{20.104}$$

Another calculated lattice sum is

$$\mu_2(\beta) = \sum_i \mathbf{x}_i^2 \langle \mathbf{S}(\mathbf{x}_i)\mathbf{S}(\mathbf{x}_j)\rangle = \sum_{k=1}^{L} h_k \beta^k, \tag{20.105}$$

which for $N = 2$ on a bcc lattice, starts out like

$$\mu_2(\beta) = 8\,\frac{\beta}{2} + 128 \cdot 56\left(\frac{\beta}{2}\right)^2 + 1412\left(\frac{\beta}{2}\right)^3 + \dots\ . \tag{20.106}$$

This diverges near the critical point like

$$\xi^5(\beta) g(\beta) \approx (\beta_c - \beta)^{-2\nu+\gamma}. \tag{20.107}$$

If we form the combination

$$X^2(\beta) \equiv \frac{\mu_2(\beta)}{6\chi(\beta)}, \tag{20.108}$$

this quantity is proportional to the square of the coherence length, and diverges like

$$X^2(\beta) \approx (\beta_c - \beta)^{-2\nu}. \tag{20.109}$$

This function gives direct access to the critical exponent ν.

In a finite system, all lattice functions such as $\chi(\beta)$ and $X^2(\beta)$ are polynomials in β. These have complex-conjugate pairs of zeros in the complex plane corresponding to the degree of the polynomials. For a growing number of lattice sites, these zeros approach the real β in the form of two sequences from above and below. In the thermodynamic limit of an infinite system, the points move arbitrarily close to each other and form two continuous lines whose end points

pinch the β-axis at β_c [22]. When taking the logarithm of Z and forming $-\beta f'$, the lines of zeros become lines of singularities, giving rise to a critical power behavior, such as

$$\chi(\beta) \propto (\beta_c - \beta)^{-\gamma}. \tag{20.110}$$

The critical exponent γ can be extracted from the power series in the following way. Expanding (20.110) in powers of β, we obtain a series

$$\chi(\beta) \propto \sum_n \binom{-\gamma}{n} \left(\frac{\beta}{\beta_c}\right)^n. \tag{20.111}$$

For the ratios R_n of two successive large order coefficients, this implies the following limit:

$$\begin{aligned} R_n &= \frac{1}{\beta_c}\binom{-\gamma}{n} \Big/ \binom{-\gamma}{n-1} = \frac{1}{\beta_c}\frac{\gamma(\gamma+1)\cdots(\gamma+n-1)}{n!} \Big/ \frac{\gamma(\gamma+1)\cdots(\gamma+n-2)}{(n-1)!} \\ &= \frac{1}{\beta_c}\left(1+\frac{\gamma-1}{n}\right). \end{aligned} \tag{20.112}$$

If an expansion is known up to a sufficiently high order in β, this can be used to estimate the critical β_c as well as the critical exponent γ. We simply plot $1/R_n$ against $1/n$ and read off β_c from the extrapolated intercept. This procedure is called the *ratio test*. The slope at the origin is $-(\gamma-1)\beta_c$, and yields the critical index γ. The plots for $N = 0$, 1, 2, and 3 are shown in Fig. 20.31. The extrapolation of the average of even and odd sequences is shown in Fig. 20.32.

Similar procedures can be applied to the power series for $X^2(\beta)$ and the critical exponent 2ν. In Fig. 20.33 we determined the critical exponent ν by plotting the ratios R_n against $1/n$, fitting the last four points of even and odd sequences by parabolas, and deducing from the average slope the critical exponent ν.

Butera and Comi have performed much more sophisticated analyses which are summarized in Tables 20.11 and 20.12 at the end of this section. For an explanation of their procedures see the original paper in Ref. [23]. Their critical exponents agree reasonably well with those in Tables 20.1 on page 375 and 20.2 on page 389.

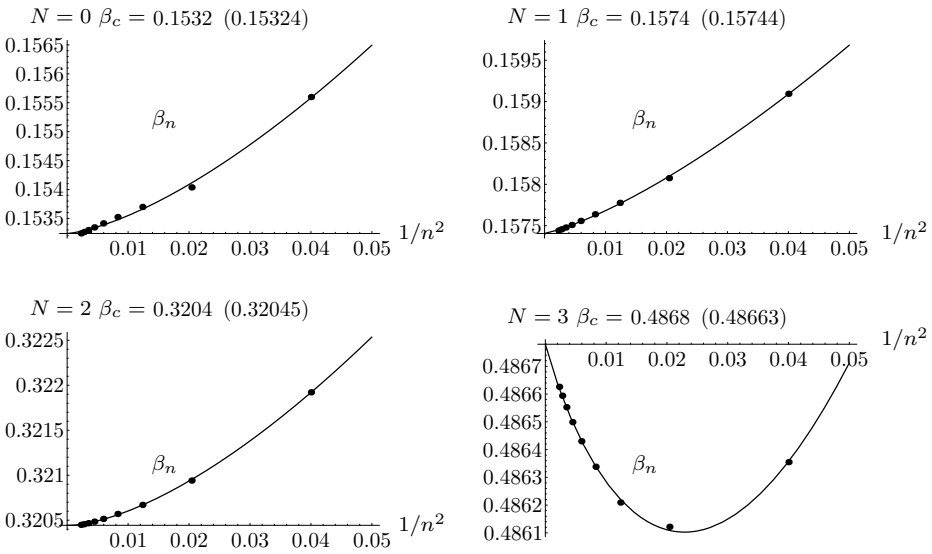

FIGURE 20.30 Critical inverse temperature β_c from a parabolic fit to the average of the even and odd sequences (20.98), plotted against $1/n^2$. The value at $1/n^2 = 0$ yields the critical β_c. The numbers in parentheses show the highest approximation to β_c before the extrapolation.

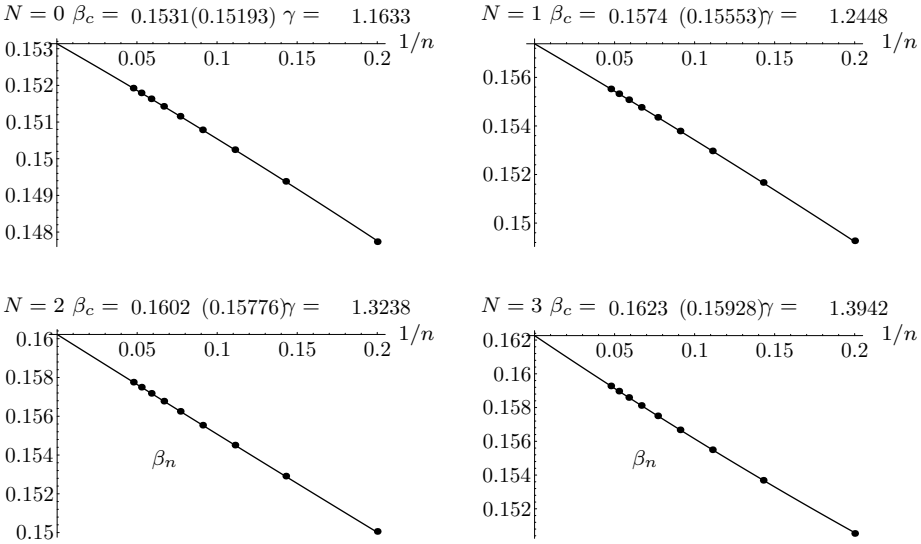

FIGURE 20.31 Critical inverse temperature β_c from the last four terms of the average of the even and odd sequences (20.98), plotted against $1/n$. An almost straight parabola is fitted through the points whose value at $1/n = 0$ yields the critical reduced temperature $t_c \equiv 1/\beta_c$. The slope at the origin is an approximation for the critical exponent γ. The numbers in parentheses show the highest approximations to β_c before the extrapolation.

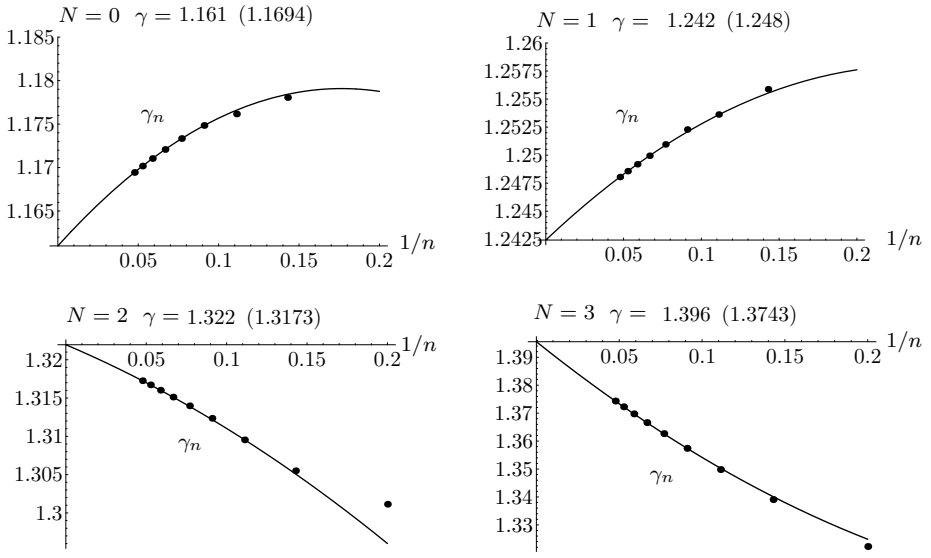

FIGURE 20.32 Critical Exponents γ from the average of the sequences (20.99) for even and odd n, plotted against $1/n$. The extrapolation curve at $1/n = 0$ yields the critical exponent γ. Only the last four averages are extrapolated parabolically.

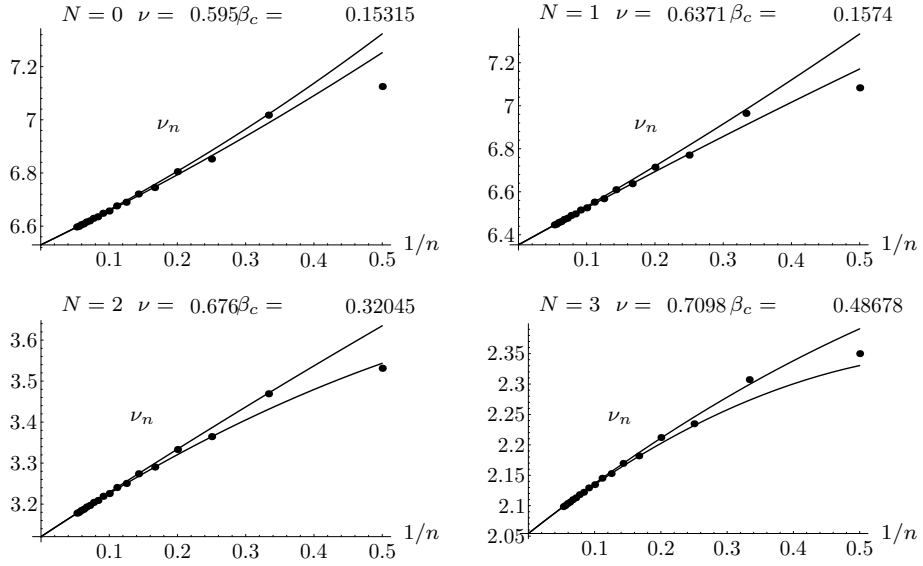

FIGURE 20.33 Critical Exponents ν from the average of the slopes of the even and odd ratios.

TABLE 20.11 Summary of lattice estimates of critical exponents for $0 \leq N \leq 3$.

N	Method and Ref.	β_c	γ	ν
0	HTE sc unbiased [24]	0.2134987(10)	1.16193(10)	
	HTE sc unbiased	0.213497(6)	1.161(2)	0.592(2)
	HTE sc θ-biased	0.213493(3)	1.1594(8)	0.5878(6)
	MonteCarlo sc [25]	0.2134969(10)		0.5877(6)
	MonteCarlo sc [26]	0.213492(1)	1.1575(6)	
	HTE bcc unbiased	0.153131(2)	1.1612(8)	0.591(2)
	HTE bcc θ-biased	0.153128(3)	1.1582(8)	0.5879(6)
	R.G. FD perturb. [12]		1.1569(8)	0.5872(8)
	R.G. $\epsilon-$expansion [27]		1.157(3)	0.5880(15)
1	HTE sc unbiased	0.221663(9)	1.244(3)	0.634(2)
	HTE sc θ-biased	$\big(0.2216544(3)\big)$	1.2388(10)	0.6315(8)
	MonteCarlo sc [28]	0.2216595(26)		0.6289(8)
	MonteCarlo sc [29]	0.2216544(3)	1.237(2)	0.6301(8)
	HTE bcc [30]		1.2395(4)	0.632(1)
	HTE bcc [31]		1.237(2)	0.6300(15)
	HTE bcc unbiased	0.157379(2)	1.243(2)	0.634(2)
	HTE bcc θ-biased	$\big(0.157373(2)\big)$	1.2384(6)	0.6308(5)
	R.G. FD perturb. [12]		1.2378(12)	0.6301(10)
	R.G. $\epsilon-$expansion [27]		1.2390(25)	0.6310(15)
2	Experiment [16]			0.6702(1)
	HTE sc unbiased	0.45419(3)	1.327(4)	0.677(3)
	HTE sc θ-biased	0.45419(3)	1.325(3)	0.675(2)
	MonteCarlo sc [32]	0.45420(2)	1.308(16)	0.662(7)
	MonteCarlo sc [33]	0.4542(1)	1.316(5)	0.670(7)
	MonteCarlo sc [34]	0.454165(4)	1.319(2)	0.672(1)
	HTE bcc unbiased	0.320428(3)	1.322(3)	0.674(2)
	HTE bcc θ-biased	0.320427(3)	1.322(3)	0.674(2)
	HTE fcc [35]	0.2075(1)	1.323(15)	0.670(7)
	R.G. FD perturb. [12]		1.318(2)	0.6715(15)
	R.G. $\epsilon-$expansion [27]		1.315(7)	0.671(5)
3	HTE sc unbiased	0.69303(3)	1.404(4)	0.715(3)
	HTE sc θ-biased	0.69305(4)	1.406(3)	0.716(2)
	MonteCarlo sc [36]	0.693035(37)	1.3896(70)	0.7036(23)
	MonteCarlo sc [34]	0.693002(12)	1.399(2)	0.7128(14)
	HTE bcc unbiased	0.486805(4)	1.396(3)	0.711(2)
	HTE bcc θ-biased	0.486820(4)	1.402(3)	0.714(2)
	MonteCarlo bcc [36]	0.486798(12)	1.385(10)	0.7059(37)
	HTE fcc [37]	0.3149(6)	1.40(3)	0.72(1)
	R.G. FD perturb. [12]		1.3926(26)	0.7096(16)
	R.G. $\epsilon-$expansion [27]		1.39(1)	0.710(7)

TABLE 20.12 Summary of lattice estimates of critical parameters for $4 \leq N \leq 12$.

N	Method and Ref.	β_c	γ	ν
4	HTE sc unbiased	0.93589(6)	1.474(4)	0.750(3)
	HTE sc θ-biased	0.93600(4)	1.491(4)	0.759(3)
	MonteCarlo sc [38]	0.9360(1)	1.477(18)	0.7479(90)
	MonteCarlo sc [34]	0.935861(8)	1.478(2)	0.7525(10)
	HTE bcc unbiased	0.65531(6)	1.461(4)	0.744(3)
	HTE bcc θ-biased	0.65542(3)	1.484(4)	0.756(3)
	R.G. FD perturb. [3]		1.449	0.738
6	HTE sc unbiased	1.42859(6)	1.582(5)	0.804(3)
	HTE sc θ-biased	1.42895(6)	1.614(5)	0.821(3)
	HTE bcc unbiased	0.99613(6)	1.566(4)	0.796(3)
	HTE bcc θ-biased	0.99644(4)	1.608(4)	0.819(3)
	R.G. FD perturb. [3]		1.556	0.790
8	HTE sc unbiased	1.9263(2)	1.656(5)	0.840(3)
	HTE sc θ-biased	1.92705(7)	1.701(4)	0.864(3)
	HTE bcc unbiased	1.33984(7)	1.644(5)	0.833(3)
	HTE bcc θ-biased	1.34040(6)	1.696(4)	0.862(3)
	R.G. FD perturb. [3]		1.637	0.830
	1/N expansion [7]		1.6449	0.8355
10	HTE sc unbiased	2.4267(2)	1.712(6)	0.867(4)
	HTE sc θ-biased	2.42792(8)	1.763(4)	0.894(4)
	HTE bcc unbiased	1.68509(8)	1.699(5)	0.860(4)
	HTE bcc θ-biased	1.68586(7)	1.761(4)	0.893(3)
	R.G. FD perturb. [3]		1.697	0.859
	1/N expansion [7]		1.7241	0.8731
12	HTE sc unbiased	2.9291(3)	1.759(6)	0.889(4)
	HTE sc θ-biased	2.9304(1)	1.812(5)	0.916(4)
	HTE bcc unbiased	2.03130(8)	1.741(6)	0.881(4)
	HTE bcc θ-biased	2.03230(8)	1.808(5)	0.914(3)
	R.G. FD perturb. [3]		1.743	0.881
	1/N expansion [7]		1.7746	0.8969

Notes and References

The individual citations in the text refer to the papers below.

[1] G. Parisi, J. Stat. Phys. **23**, 49 (1980).

[2] Expansions up to six loops for all O(N) were calculated in
G.A. Baker, Jr., B.G. Nickel, and D.I. Meiron, Phys. Rev.B **17**, 1365 (1978).
More details are containeed in an unpublished report
B.G. Nickel, D.I. Meiron, and G.A. Baker, Jr., University of Guelph report, 1977 .
A copy of this report can be downloaded in PDF format from our Berlin server starting at www.physik.fu-berlin.de/˜kleinert/re.html#b8.

[3] S.A. Antonenko and A.I. Sokolov, Phys. Rev. E **51**, 1894 (1995); Fiz. Tverd. Tela (Leningrad) **40**, 1284 (1998) [Sov. Phys. Sol. State **40**, 1169 (1998)].

[4] See the remark at the end of
G.A. Baker, Jr., B.G. Nickel, M.S. Green, and D.I. Meiron, Phys. Rev. Lett. **36**, 1351 (1976).

[5] J.A. Gracey, *Progress with Large-Nf β-Functions*, Talk presented at 5th International Workshop on Software Engineering, Neural Nets, Genetic Algorithms, Expert Systems, Symbolic Algebra and Automatic Calculations, Lausanne, Switzerland, 2-6th September, 1996, publ. in Nucl. Instrum. Meth. A **389**, 361 (1997) (hep-th/9609409).
See also
D.J. Broadhurst, J.A. Gracey, and D. Kreimer, Z. Phys. C **75**, 559 (1997) (hep-th/9607174).
S.E. Derkachov, J.A. Gracey, and A.N. Manashov, Eur. Phys. J. C **2**, 569 (1998) (hep-ph/9705268).

[6] A.N. Vasil'ev, Yu.M. Pis'mak, and J.R. Honkonen, Theor. Math. Phys. **50**, 127 (1982).

[7] Y. Okabe and M. Oku, Prog. Theor. Phys. **60**, 1287 (1978).

[8] H. Kleinert, Phys. Rev. D **57**, 2264 (1998) (E-Print aps1997jun25_001); addendum (cond-mat/9803268); See also H. Kleinert, Phys. Lett. B **434**, 74 (1998) (cond-mat/9801167).

[9] J.C. Le Guillou and J. Zinn-Justin, Phys. Rev. B **21**, 3976 (1980); Phys. Rev. Lett. **39**, 95 (1977).

[10] S.G. Gorishny, S.A. Larin, and F.V. Tkachov, Phys. Lett. A **101**, 120 (1984).
The critical exponents obtained there are based on the ε-expansions calculated in
A.A. Vladimirov, D.I. Kazakov, and O.V. Tarasov, Zh. Eksp. Teor. Fiz. **77**, 1035 (1979) [Sov. Phys. JETP **50**, 521 (1979)];
K.G. Chetyrkin, S.G. Gorishny, S.A. Larin, and F.V. Tkachov, Phys. Lett. B **132**, 351 (1983);
K.G. Chetyrkin, A.L. Kataev, and F.V. Tkachov, Phys. Lett. B **99**, 147 (1981); **101**, 457 (1981);
D.I. Kazakov, *ibid.* **133**, 406 (1983). The recent corrections of their five-loop expansion coefficients in
H. Kleinert, J. Neu, V. Schulte-Frohlinde, K.G. Chetyrkin, S.A. Larin, Phys. Lett. B **272**, 39 (1991) (hep-th/9503230); Erratum ibid. **319**, 545 (1993) have only little effects on these results.

[11] J.C. Le Guillou and J. Zinn-Justin, J. de Phys. Lett **46**, L137 (1985). Their expansion coefficients are the same as in [10].

[12] D.B. Murray and B.G. Nickel, *Revised estimates for critical exponents for the continuum N-vector model in 3 dimensions*, Unpublished Guelph University report (1991).

[13] In contrast to Eqs. (20.12) and (20.13), the numbers on the right are now the true coefficients, i.e., we have *not* suppressed a factor $(N+8)^7$ accompanying the power $\bar{g}^7$, to save space.

[14] R. Guida, J. Zinn-Justin, J. Phys. **A 31**, 8103 (1998) (cond-mat/9803240).

[15] The instanton action and the numbers in Tables 20.3 and 20.4 were first calculated in Ref. [1].

[16] J.A. Lipa, D.R. Swanson, J. Nissen, T.C.P. Chui, and U.E. Israelson, Phys. Rev. Lett. **76**, 944 (1996).
The initially published fit to the data was erroneous and corrected in a footnote (number [15]) of a subsequent paper
J.A. Lipa, D.R. Swanson, J. Nissen, Z.K. Geng, P.R. Williamson, D.A. Stricker, T.C.P. Chui, U.E. Israelson, and M. Larson, Phys. Rev. Lett. **84**, 4894 (2000).

[17] For a discussion of such contributions see
B.G. Nickel, Physica A **177**, 189 (1991);
A. Pelissetto and E. Vicari, Nucl. Phys. B **519**, 626 (1998);
522, 605 (1998); Nucl. Phys. Proc. Suppl. **73**, 775 (1999). See also the review article by these authors in cond-mat/0012164.

[18] H. Kleinert, Phys. Lett. B **360**, 65 (1995) (quant-ph/9507009).

[19] H. Kleinert, Phys. Lett. A **277**, 205 (2000) (cond-mat/9906107).

[20] H. Kleinert, Phys. Rev. D **60**, 085001 (1999) (hep-th/9812197).

[21] See the book by
H.E. Stanley, *Introduction to Phase Transitions and Critical Phenomena*, Oxford Science Publications, Oxford, 1971;
or
H. Kleinert, *Gauge Fields in Condensed Matter*, World Scientific, Singapore, 1989, Vol. I, *Superflow and Vortex Lines, Disorder Fields and Phase Transitions*, Sections 4.5 and 9.5 (www.physik.fu-berlin.de/˜kleinert/re.html#b1).

[22] C. Itzykson, R.B. Pearson, J.-B. Zuber, Nucl. Phys. B **220**, 415 (1983).

[23] P. Butera and M. Comi, Phys. Rev. B **56**, 8212 (1997) (hep-lat/973018).

[24] D. MacDonald, D.L. Hunter, K. Kelly and N. Jan, J. Phys. A **25**, 1429 (1992).

[25] B. Li, N. Madras and A.D. Sokal,, J. Stat. Phys. **80**, 661 (1995).

[26] S. Caracciolo, M.S. Causo and A. Pelissetto, cond-mat/9703250.

[27] J. Zinn-Justin, *Quantum field theory and critical phenomena* (Clarendon, Oxford, 1989, third edition 1996).

[28] A.M. Ferrenberg and D.P. Landau, Phys. Rev. B **44**, 5081 (1991).

[29] H.W.J. Blöte, E. Luijten and J.R. Heringa, J. Phys. A **28**, 6289 (1995); A.L. Talapov and H.W.J. Blöte, J. Phys. A **29**, 5727 (1996).

[30] J.H. Chen, M.E. Fisher and B.G. Nickel, Phys. Rev. Lett. **48**, 630 (1982); M.E. Fisher and J.H. Chen, J. Physique **46**, 1645 (1985).

[31] B.G. Nickel and J.J. Rehr, J. Stat. Phys. **61**, 1 (1990).

[32] M. Hasenbusch and S. Meyer, Phys. Lett. B **241**, 238 (1990);
A.P. Gottlob and M. Hasenbusch , Physica A **201**, 593 (1993).

[33] W. Janke, Phys. Lett. A **143**, 306 (1990).

[34] H.G. Ballesteros, L.A. Fernandez, V. Martin-Mayor and A. Muñoz-Sudupe, Phys. Lett. B **387**, 125 (1996).

[35] M. Ferer, M.A. Moore and M. Wortis, Phys. Rev. B **8**, 5205 (1973).

[36] K. Chen, A.M. Ferrenberg and D.P. Landau, Phys. Rev. B **48**, 3249 (1993); J. Appl. Phys., **73**, 5488 (1993);
C. Holm and W. Janke, Phys. Lett. A **173**, 8 (1993) and Phys. Rev. B **48**, 936 (1993).

[37] D.S. Ritchie and M.E. Fisher, Phys. Rev. B **5**, 2668 (1972);
S. McKenzie, C. Domb and D.L. Hunter, J. Phys. A **15**, 3899 (1982);
M. Ferer and A. Hamid-Aidinejad, Phys. Rev. B **34**, 6481 (1986).

[38] K. Kanaya and S. Kaya, Phys. Rev. D **51**, 2404 (1995).

Several interesting papers appeared after this chapter was written:
M. Campostrini, A. Pelissetto, P. Rossi, E. Vicari, Phys. Rev. E **60**, 3526 (1999); Phys. Rev. B **61**, 5905 (2000),
the latter producing a number for the critical exponent α of the specific heat in superfluid helium very close to our result from strong-coupling theory in the paper cited in Ref. [19], whose results are contained in Section 20.7.
Recent Monte Carlo studies are
M. Weigel and W. Janke, *High-precision Monte Carlo study of universal correlation lengths scaling in three-dimensional O(n) spin models*, Leipzig preprint March 2000 (cond-mat/0003124);
H.W.J. Blöte, J.R. Heringa, M.M. Tsypin, *Three-dimensional Ising model in the fixed-magnetization ensemble: a Monte Carlo study* (cond-mat/9910145).
There are also interesting new results in
P. Butera and M. Comi, Phys. Rev. B **60**, 6749 (1999) (hep-lat/9903010); Phys. Rev. B **50**, 3052 (1994) (cond-mat/9902326); Phys. Rev. B **58**, 11552 (1998).

Recently, accurate five-loop studies appeared for two-dimensional ϕ^4 theories. Extending the perturbation expansions for a single real field in Ref. [2] to any O(N), the critical exponents were calculated by
E.V. Orlov and A.I. Sokolov, *Critical thermodynamics of the two-dimensional systems in five-loop renormalization-group approximation*, Fiz. Tverdogo Tela, **42** (2000), November issue (hep-th/0003140).